Neural circuitry for maternal oxytocin release induced by infant cries

Silvana Valtcheva[1-5,7*], Habon A. Issa[1-5,7], Chloe J. Bair-Marshall[1-5], Kathleen A. Martin[1-5], Kanghoon Jung[6], Yiyao Zhang[2], György Buzsáki[2], Hyung-Bae Kwon[6] and Robert C. Froemke[1-5*]

[1] Skirball Institute for Biomolecular Medicine, New York University School of Medicine, New York, NY 10016, USA.

[2] Neuroscience Institute, New York University School of Medicine, New York, NY 10016 USA.

[3] Department of Otolaryngology, New York University School of Medicine, New York, NY 10016, USA.

[4] Department of Neuroscience and Physiology, New York University School of Medicine, New York, NY 10016, USA.

[5] Center for Neural Science, New York University, New York, NY 10003, USA.

[6] Solomon H. Snyder Department of Neuroscience, Johns Hopkins University School of Medicine, Baltimore, MD 21205, USA.

[7] These authors contributed equally.

* Correspondence: silvana.valtcheva@uk-koeln.de and robert.froemke@med.nyu.edu

Summary

Oxytocin is a neuropeptide important for maternal physiology and childcare, including parturition and milk ejection during nursing. Suckling triggers oxytocin release, but other sensory cues- specifically infant cries- can elevate oxytocin levels in new human mothers indicating that cries can activate hypothalamic oxytocin neurons. Here we describe a neural circuit routing auditory information about infant vocalizations to mouse oxytocin neurons. We performed in vivo electrophysiological recordings and photometry from identified oxytocin neurons in awake maternal mice presented with pup calls. We found that oxytocin neurons responded to pup vocalizations, but not pure tones, via input from the posterior intralaminar thalamus, and repetitive thalamic stimulation induced lasting disinhibition of oxytocin neurons. This circuit gates central oxytocin release and maternal behavior in response to calls, providing a mechanism for the integration of sensory cues from the offspring in maternal endocrine networks to ensure modulation of brain state for efficient parenting.

Keywords

auditory circuit, hypothalamus, infant cries, maternal behavior, oxytocin, long-term plasticity, nursing, thalamus

Introduction

Parenting behaviors emerge from complex neural circuits, which must confer sensitivity to infant needs to ensure survival of the species. One important molecular signal for the maternal brain is oxytocin, a nine amino acid peptide produced mainly in the paraventricular nucleus (PVN) and supraoptic nucleus of the hypothalamus (Freund-Mercier et al., 1988; Lyons and Broberger, 2014; Grinevich et al., 2016; Althammer and Grinevich, 2017; Jurek and Neumann, 2018; Valtcheva and Froemke, 2019; Froemke and Young, 2021). Peripheral oxytocin is absolutely required for milk ejection during nursing and important for uterine contractions during labor, whereas oxytocin release in the central nervous system seems to be involved in a wide range of behaviors including reproduction, parental care, pair bonding, and empathy (Neumann and Landgraf, 2012; Dulac et al., 2014; Rilling and Young, 2014; Feldman, 2016; Uvnas-Moberg et al., 2020).

Oxytocin is believed to powerfully enhance pro-social and parental behavior by acting to increase the salience of social cues such as infant cries (Swain et al., 2014; Dölen, 2015; Grinevich and Stoop, 2018; Froemke and Young, 2021). Amplification of these sensory signals via central oxytocin release might increase behavioral motivation to engage in social interactions and maternal care. However, there is limited information about the neural pathways conveying sensory information to hypothalamic oxytocin neurons. In female rodents, oxytocin neurons are thought to be activated by somatosensory stimuli during nursing or parturition, relayed from the periphery through spinal cord and brainstem circuits (Wakerley and Lincoln, 1973; Summerlee, 1981; Summerlee and Lincoln, 1981; Belin and Moos, 1986; Neumann et al., 1993; Brown and Moos, 1997; Leng et al., 1999; Valtcheva and Froemke, 2019). In humans, baby cries are among the most powerful sounds we hear, and most nursing mothers respond to cries with increased hypothalamic

activity, elevations of plasma oxytocin levels, increased infant contact and comforting behaviors, and occasional milk ejection (McNeilly et al., 1983; Lorberbaum et al., 2002; Swain et al., 2014; Bornstein et al., 2017). However, many mothers- particularly first-time mothers and women suffering from postpartum conditions- struggle to breastfeed their infants, have decreased sensitivity to infant cries, and impaired caregiving responses. Human studies suggest that these complications might relate to decreased oxytocin levels (Kim et al., 2014; Swain et al., 2014; Esposito et al., 2017; Pawluski et al., 2017), underscoring the importance of understanding the mechanisms by which infant cues activate oxytocin neurons.

Oxytocin neurons of the PVN receive projections from many brain areas (Brown et al., 2013; Tang et al., 2020), but it is unknown which specific circuits relay auditory information. PVN and the surrounding hypothalamic nuclei represent a dense and heterogeneous area with interspersed neuronal populations, of which only a fraction are oxytocinergic (Althammer and Grinevich, 2017; Romanov et al., 2017; Murakami et al., 2018). It has therefore been historically challenging to make recordings from unambiguously identified oxytocin neurons. Recent studies using optogenetic phototagging or Ca^{2+} imaging methods have successfully recorded from identified PVN oxytocin neurons in non-parental female and male rodents in vivo (Hung et al., 2017; Carcea et al., 2019; Resendez et al., 2020; Tang et al., 2020), showing that these cells can be activated during social interactions. Other hypothalamic cell types possibly receive information about non-somatic sensory input as well, such as activation of CRH neurons by visual stimuli (Daviu et al., 2020). Here we take advantage of these new approaches, performing electrophysiological cell-attached and whole-cell recordings from hypothalamic neurons (Bourque and Renaud, 1991; Katz et al., 2013; Muñoz et al., 2014, 2017; Branco et al., 2016), combined with fiber photometry, viral

tracing, and studies of synaptic transmission and plasticity in brain slices to determine if and how mouse pup distress calls might activate maternal PVN oxytocin neurons.

Activating hypothalamic oxytocin neurons by infant cries should increase oxytocin release throughout the central nervous system, perhaps serving as an urgency signal and motivational cue to promote maternal behaviors. One important form of mouse maternal behavior is retrieval of pups to the nest, triggered by distress vocalizations produced by isolated infants (Ehret, 2005; Liu et al., 2006; Tasaka et al., 2020). Oxytocin signaling to the auditory cortex is important for promoting synaptic plasticity leading to enhanced detection of pup calls and retrieval behavior (Marlin et al., 2015; Carcea et al., 2019; Schiavo et al., 2020; Tasaka et al., 2020). PVN oxytocin neurons also send projections to a variety of other brain structures implicated in maternal care and social behavior (Dölen, 2015; Althammer and Grinevich, 2017; Grinevich et al., 2016; Lewis et al., 2020; Tang et al., 2020; Zhang et al., 2020). These include sensory, limbic, and motivational areas such as the ventral tegmental area (VTA), a brain region involved in rewarding aspects of maternal behavior, maternal motivation, and pup retrieval (Numan, 2006; Numan and Young, 2016; Fang et al., 2018; Kohl and Dulac, 2018; Rincón-Cortés and Grace, 2020). However, there are limited data on measuring endogenous oxytocin release, particularly in the central nervous system in vivo, in part confounded by the potential for co-release of other neurotransmitters aside from oxytocin by PVN oxytocinergic axons (Jameson et al., 2014; Chini et al., 2017; Ryan et al., 2017). To ask if a specific call-sensitive circuit contributes to maternal care and central oxytocin release, we assessed behavioral pup retrieval with chemogenetics and utilized a novel genetically-encoded oxytocin sensor (Mignocchi et al., 2020) to measure endogenous oxytocin signaling in the VTA.

Results

PVN oxytocin neurons are persistently activated by pup distress vocalizations

We first recorded from PVN oxytocin neurons in awake head-fixed mouse dams. To specifically target oxytocin neurons in vivo, we used channelrhodopsin2-assisted patching (Katz et al., 2013; Muñoz et al., 2014, 2017) in awake Oxytocin:Cre x Ai32 mice (**Figures 1A and B**), and made cell-attached and whole-cell recordings from channelrhodopsin2-expressing oxytocin neurons (ChR2+; OT+) and other optically-unresponsive PVN neurons (ChR2-; OT-). Oxytocin neurons were identified by reliable spiking responses to brief pulses of blue light (**Figures 1C and S1**), elicited by short blue light pulses (50 ms; **Figures S1A and B**) or long pulses (200 ms; **Figures S1C-G**) at various laser powers. Recordings from ChR2+ (OT+) and ChR2- (OT-) neurons were made at similar depths from the pial surface, and had baseline firing rates (**Figure 1D**) comparable to those previously reported for extracellular recordings of PVN neurons in rodents (Wakerley and Lincoln, 1973; Summerlee and Lincoln, 1981; Belin and Moos, 1986; Brown and Moos, 1997) including recent studies of optically-identified oxytocin cells (Carcea et al., 2019; Tang et al., 2020).

To investigate whether ChR2+ (OT+) and/or ChR2- (OT-) neurons are activated by pup distress vocalizations, we measured 1-2 min of baseline spiking ('Pre') followed by repetitive presentation of a set of 15-18 distress calls recorded from isolated pups ('Calls', each one-second call followed by one second of silence for a total duration of ~30-40 s), and assessed changes in ongoing activity thereafter for the duration of the recordings ('Post'). We found that pup call presentation increased the firing rates of ChR2+ (OT+) neurons (Pre: 2.9±0.7 Hz, Post: 5.0±1.6 Hz, p=0.001, n=12 cells from N=6 dams), but ChR2- (OT-) neuron firing was unaltered by calls (Pre: 3.1±0.9 Hz, Post:

3.6±1.0 Hz, p=0.07, n=11, N=5; **Figures 1E-H and S2A and B**). On average, pup calls increased the firing rate of ChR2+ (OT+) neurons to 227±42.8% of baseline (p=0.01), while the firing of ChR2- (OT-) neurons was not significantly affected (121.8±12.7% of baseline, p=0.12, **Figures 1I and J**). Increased activity of ChR2+ (OT+) neurons lasted for 2+ minutes after stimulus onset, but this enhancement was not observed during call presentation itself (**Figures 1G-I and S2C-F**). The sustained increase in oxytocin neuron firing was specific to pup calls, as PVN neurons did not respond to pure tones (**Figure S2G-I**). These results show that pup vocalizations can activate PVN oxytocin neurons, but not with stimulus-locked responses such as those typically observed in the central auditory system including the auditory cortex (Liu et al., 2006; Liu and Schreiner, 2007; Cohen et al., 2011; Cohen and Mizrahi, 2015; Marlin et al., 2015; Shepard et al., 2016; Tasaka et al., 2018, 2020). Instead, oxytocin cells require more prolonged stimulus periods to increase activity, perhaps as might naturally occur before and during episodes of maternal care.

We performed fiber photometry of oxytocin neuronal responses in awake head-fixed dams to examine if the population-level activity was also enhanced after pup calls. We injected AAVDJ-CAG-FLEx-GCaMP6s in the PVN of Oxytocin:Cre dams and implanted an optical fiber just above PVN (**Figure 2A**). After waiting 2-3 weeks for expression, we measured changes in GCaMP6s signals in oxytocin neurons of head-fixed dams while playing pup distress calls (**Figure 2B**). We played five sets of pup calls (x15 calls each, 1 second gap in between calls) separated by 1-3 minutes and observed substantial responses after each set of calls (2.3±3.8, p=0.016, N=4 dams; **Figures 2C-F**). Thus, despite potential heterogeneity in the hypothalamic single-cell responses, pup calls trigger a collective activation of oxytocin neurons for an extended duration.

PVN oxytocin neurons receive projections from the auditory thalamus

What projections relay information about incoming signals such as vocalizations and pup distress cues to PVN oxytocin neurons? Especially given the absence of phase-locked responses to pup calls and pure tones-evoked activity, we reasoned that it was unlikely that PVN neurons were receiving direct input from classical auditory relays, e.g., cochlear nucleus or the auditory cortex. To more thoroughly map which auditory areas project to PVN oxytocin neurons, we used *Cre*-inducible, retrograde pseudotyped monosynaptic rabies virus (Wickersham et al., 2007) to determine the inputs to these cells. We targeted oxytocin neurons by injecting AAV2-EF1a-FLEX-TVA-GFP in the PVN of Oxytocin:Cre dams followed by an injection of SADΔG-mCherry two weeks later (**Figures 3A and B**, N=4 dams). Consistent with our hypothesis, most auditory areas did not send direct projections to the PVN; we did not detect retrograde rabies infection and mCherry staining in the medial geniculate body of the thalamus (MGB; **Figure 3C**), auditory cortex (AuCx; **Figure 3D**), or the inferior colliculus (IC; **Figure 3E**). However, we did observe dense and reliable rabies-based mCherry staining in the posterior intralaminar nucleus of the thalamus (PIL; **Figure 3C**). We conclude that PIL provides a major monosynaptic input to oxytocin neurons in the PVN.

PIL is part of the non-lemniscal auditory pathway, as one of the nuclei of the paralaminar complex of the thalamus which also includes the suprageniculate nucleus, the medial division of the medial geniculate body and the peripeduncular nucleus. PIL is a multimodal thalamic nucleus implicated in maternal and social behaviors (Hansen and Köhlerb, 1984; Factor et al., 1993; Cservenák et al., 2010, 2013, 2017; Dobolyi et al., 2018). This brain region also receives direct projections from the IC and AuCx (LeDoux et al., 1987; Yasui et al., 1990; Linke, 1999; Cai et al., 2018), and previous

studies have found that PIL neurons can respond to synthetic sounds (Bordi and LeDoux, 1994a, 1994b; Palkovits et al., 2004).

We next asked if PIL neurons are also activated by pup calls. We found reliable c-fos staining in the PIL (N=3 dams) of wild-type dams after playback of pup calls (**Figures S3A and B**). As expected, some cells in MGB were also labeled for c-fos, as these cells are likely driven by acoustic features within the pup calls. We performed multiunit recordings from awake wild-type dams to measure auditory responses in PIL in vivo (**Figures S3C-F**). PIL multiunit spiking activity increased during the duration of the calls from 24.8±3.0 Hz to 31.6±2.9 Hz (p=0.03, N=6 dams; **Figure S3E**) which corresponded to 130.5±8.7 % of baseline (p=0.02; **Figure S3F**). These PIL recording sites also responded to ultrasonic pure tones (23-64 kHz; **Figures S3G and H**), as previously described (Bordi and LeDoux, 1994a, 1994b).

We asked if PIL receives functional synaptic inputs from the IC and AuCx, two major auditory areas that respond to pup calls. We tested the strength of these synaptic connections using channelrhodopsin2-assisted circuit mapping (Petreanu et al., 2007; Livneh et al., 2017). We injected AAV1-hSyn-hChR2(H134R)-EYFP in the IC (**Figure 3F and G**) or AuCx (**Figure 3H and I**) of wild-type dams, and performed whole-cell voltage-clamp recordings from PIL neurons in acute brain slices while optogenetically stimulating axons from either IC or AuCx. When stimulating IC terminals in PIL, we observed optogenetically-induced EPSCs (oEPSCs) in 10 out of 12 PIL neurons, indicating that PIL receives reliable synaptic inputs from IC (**Figure 3G**). In contrast, when we tested inputs from the AuCx in PIL neurons, only 4 out of 13 neurons were connected (**Figure 3I**), suggesting that AuCx synapses onto PIL neurons are sparser than IC

synapses. These findings are similar to those in other neurons in the paralaminar thalamus, such as neurons in the medial part of the MGB, which are more efficiently driven by inputs from IC than AuCx (Smith et al., 2007).

We then examined the synaptic connections between PIL and PVN oxytocin neurons. Previous studies have identified anatomical connections between PIL and PVN (Campeau and Watson, 2000; Dobolyi et al., 2003; Cservenák et al., 2017; Tang et al., 2020), and so here we functionally tested the strengths of these putative inputs. We injected AAV1-hSyn-hChR2(H134R)-EYFP in PIL of Oxytocin:Cre x Ai9 dams, to perform in vitro whole-cell voltage-clamp recordings from identified oxytocin neurons (expressing tdTomato) in acute brain slices of PVN while optogenetically stimulating PIL terminals (**Figure 3J**). We observed reliable oEPSCs in the majority of oxytocin cells (49/62 connections) indicating that oxytocin neurons receive strong connections from PIL with high probability (**Figure 3K**). We did not observe any EYFP staining of synaptic terminals in PVN, originating from IC or AuCx, when injecting wild-type dams with AAV1-hSyn-hChR2(H134R)-EYFP in the IC or AuCx, respectively, further confirming that these areas do not project to PVN (**Figures S3I and J**). In summary, our findings describe a noncanonical auditory circuit that could relay pup vocalization signals via IC and AuCx via PIL to PVN oxytocin neurons.

Activation of PIL inputs to PVN decreases inhibition in oxytocin neurons

We wondered what candidate synaptic or cellular mechanisms might underlie the persistent activation of PVN oxytocin neurons elicited by pup distress calls. We considered three main hypotheses: 1) increased drive from upstream areas such as PIL, 2) changes in intrinsic excitability

of oxytocin neurons, and 3) pre- or postsynaptic forms of synaptic plasticity. To determine if the long-term increase in oxytocin neuron activity was due to increased PIL output, we performed in vivo cell-attached recordings from PIL neurons in wild-type dams, and played a set of 15 pup distress calls (**Figure S4A and B**). In general, there was no sustained increase in the spontaneous firing rate of individual PIL cells after playback of pup calls (**Figures S4C-E**), making it unlikely that persistent activation of PVN oxytocin neurons resulted from increased PIL output following pup calls (ruling out the first candidate hypothesis).

We then asked if increased firing of PVN oxytocin neurons could be caused by changes of intrinsic excitability. We injected AAV1-hSyn-hChR2(H134R)-EYFP in the PIL of Oxytocin:Cre x Ai9 dams, and performed whole-cell current-clamp recordings from identified oxytocin neurons (tdTomato+) in acute brain slices of PVN (**Figure S5A and B**). For these experiments, we used a stimulation pattern emulating PIL responses in vivo during pup call playback. Specifically, we optogenetically stimulated PIL terminals in PVN ('PIL opto') at 30 Hz for one second and repeated this high-frequency activation every two seconds for three minutes. There were no differences in the excitability of oxytocin neurons before and after PIL optical stimulation, as measured by the number of spikes elicited via intracellular current injection (**Figure S5C and D**). There were also no differences in rheobase, resting membrane potential, or input resistance of oxytocin neurons following PIL opto (**Figures S5E-G**). Together, these data indicate that increased output of PVN oxytocin neurons in vivo is not due to changes of intrinsic properties following activation of PIL inputs (ruling out the second candidate mechanistic hypothesis).

We then asked if repetitive PIL stimulation led to lasting changes in excitatory or inhibitory inputs onto PVN oxytocin neurons. For example, a reduction of inhibition could increase output of these cells. PVN is heavily innervated by inhibitory networks, and approximately half of the synapses in PVN are GABAergic (Decavel and van den Pol, 1990; Johnson et al., 2018) with both local and longer-range origins (Roland and Sawchenko, 1993; Tasker and Dudek, 1993; Larsen et al., 1994; Boudaba et al., 1996). We performed whole-cell voltage-clamp recordings of oxytocin neurons in PVN brain slices and monitored excitatory and inhibitory postsynaptic currents (EPSCs and IPSCs) evoked by a nearby extracellular stimulation electrode, before and after PIL opto (**Figure 4A and B**). While EPSCs were unaffected (**Figures 4C and D**), the amplitudes of IPSCs were significantly decreased 15+ minutes following PIL opto (**Figure 4E and F**). Correspondingly, this long-term depression of inhibition (iLTD) decreased the IPSC/EPSC ratio for oxytocin neurons (**Figure 4G**).

We hypothesized that decreased inhibition from iLTD could enhance the spiking output of oxytocin neurons. We made whole-cell current-clamp recordings from oxytocin neurons in PVN brain slices. We evoked EPSPs or single action potentials in oxytocin cells via an extracellular electrode (**Figure 4H**). The spiking output of oxytocin neurons in response to pulses of electrical stimulation significantly increased following PIL opto ('Post'; **Figures 4I and J**). Thus, repetitive PIL activation onto PVN oxytocin neurons leads to a rapid and enduring increase in spike generation via iLTD, with a similar timescale as the changes in oxytocin neuron firing in vivo after repetitive pup call presentation.

iLTD in oxytocin neurons is due to postsynaptic NMDAR-dependent internalization of $GABA_A$Rs via dynamin

Long-term reductions in inhibitory transmission can be mediated by different mechanisms. One possible pathway in the hypothalamus is decreasing inhibition via activation of presynaptic type-III metabotropic glutamate receptors (mGluRs) located on GABAergic terminals (Schrader and Tasker, 1997; Piet et al., 2003, 2004; Panatier et al., 2004). Another set of mechanisms involves presynaptic NMDA receptors (NMDARs) acting on presynaptic GABA release (Paquet and Smith, 2000), or postsynaptic NMDARs regulating cell excitability (Fleming et al., 2011; Naskar and Stern, 2014) or $GABA_A$ receptors ($GABA_A$Rs; Potapenko et al., 2013). Postsynaptic NMDARs have also been reported to trigger somatodendrtic oxytocin release and reduction of inhibition via different mechanisms (Brussaard et al., 1996; de Kock et al., 2003, 2004; Ludwig and Leng, 2006; Oliet et al., 2007; Owen et al., 2013; Mitre et al., 2016; Xiao et al., 2017; Tirko et al., 2018; Brown et al., 2020).

We first tested the involvement of type-III mGluRs in iLTD. Type-III mGluRs are not tonically activated in dams but can inhibit GABAergic transmission by a heterosynaptic mechanism in a frequency-dependent way (Piet et al., 2003, 2004). High-frequency discharge of PIL during pup calls could therefore mediate intersynaptic crosstalk between PIL inputs and inhibitory inputs onto PVN oxytocin neurons. However, the type-III mGluR antagonist MAP4 (250 μM) did not prevent iLTD induction (**Figures S6A and B**), indicating that mGluR activation is unlikely to be responsible for the enhanced oxytocin neuron firing after pup call playback.

Next, we explored if iLTD relies on pre- or postsynaptic NMDAR signaling. To ask if PIL activity can recruit postsynaptic NMDARs, we made whole-cell voltage-clamp recordings of PVN oxytocin neurons at +40 mV and monitored postsynaptic responses to optogenetic stimulation of PIL fibers. We observed outward oEPSCs, which were blocked by bath-application of the NMDAR antagonist AP5 (50 µM, p=0.02; **Figure 5A**). Furthermore, both bath-application of AP5, or intracellular delivery of use-dependent NMDAR blocker MK801 (i-MK801, 1 mM) via recording pipette abolished iLTD after PIL opto (**Figures 5B-E**). These results show that iLTD of oxytocin neurons relies on postsynaptic NMDARs. Oxytocin release downstream of NMDAR activation was not involved, as application of the oxytocin receptor antagonist OTA (1 µM) did not prevent iLTD (**Figures S6C and D**). Blockade of iLTD by NMDAR antagonists also prevented changes in IPSC/EPSC ratios (**Figures S6E and F**).

Finally, we tested if iLTD involves regulation of postsynaptic $GABA_A$Rs. Previous studies showed that NMDAR signaling can trigger dynamin-dependent internalization of postsynaptic $GABA_A$Rs (Herring et al., 2005; Vithlani et al., 2011), which might lead to iLTD via Ca^{2+}-based signal transduction cascades and reduction of functional $GABA_A$Rs (Lu et al., 2000; Sun and Liu, 2007; Haucke et al., 2011; Bannai et al., 2015). Indeed, we found that iLTD and change in IPSC/EPSC ratio were blocked by infusing the postsynaptic oxytocin neuron with a membrane-impermeable dynamin inhibitory peptide (i-Dynamin inhibitor; 1.5 mM) through the recording pipette (**Figures 5F-I, S6G and H**). These findings suggest that PIL opto rapidly triggers iLTD in oxytocin neurons by postsynaptic NMDAR-mediated internalization of $GABA_A$Rs.

PIL projections to PVN control pup retrieval behavior

Increased firing of oxytocin neurons after iLTD could have substantial impact on maternal behavior. PIL is implicated in several aspects of maternal behavior such as pup retrieval, maternal aggression and nursing (Factor et al., 1993; Dobolyi et al., 2018) which also rely on oxytocin signaling (Valtcheva and Froemke, 2019). Specifically, dams with PIL lesions have longer latencies to retrieve pups (Factor et al., 1993). We therefore asked if chemogenetic suppression of PIL input to PVN would affect pup retrieval. We virally expressed the inhibitory hM4Di receptor or a control AAV expressing mCherry in PVN-projecting PIL neurons, injecting wild-type dams with AAVrg-ENN.AAV.hSyn.Cre.WPRE.hGH in PVN and AAV8-hSyn-DIO-hM4D(Gi)-mCherry or AAV8-hSyn-DIO-mCherry in PIL (**Figures 6A and B**). We validated that bath application of clozapine N-oxide hydrochloride (CNO; 1 μM) efficiently reduced neuronal activity in PIL brain slices (**Figures 6C-E**). We then tested pup retrieval behavior in dams injected with either hM4Di or mCherry control virus and administered i.p. with saline or CNO. When hM4Di dams were administered CNO, they had significantly higher latencies to retrieve pups (**Figure 6F**), but mCherry dams were unimpaired by CNO. Although latency to retrieve pups was longer, the overall probability of retrieval was unaffected by CNO administration in both hM4Di and mCherry dams (**Figure 6G**). These results indicate that auditory input from PIL to PVN can enhance the salience of pup cues for ensuring that maternal behavior is rapid and reliable.

Pup calls induce central oxytocin release

Finally, does activation of PVN oxytocin neurons by pup calls lead to bona fide oxytocin release in other brain areas? PVN oxytocin neurons send projections to variety of brain regions including the VTA (Dölen, 2015; Grinevich et al., 2016; Althammer and Grinevich, 2017; Tang et al., 2020;

Zhang et al., 2020), which is important for rewarding aspects of maternal behavior, maternal motivation, and pup retrieval (Numan, 2006; Numan and Young, 2016; Fang et al., 2018; Kohl and Dulac, 2018; Rincón-Cortés and Grace, 2020). Pharmacological inactivation of VTA or disruption of dopaminergic signaling impairs pup retrieval (Hansen et al., 1991; Numan et al., 2009). Oxytocin receptor activation increases activity of VTA dopamine neurons (Shahrokh et al., 2010; Xiao et al., 2017, 2018) and blocking VTA oxytocin signaling impacts pup retrieval (Pedersen et al., 1994). Despite this evidence for central oxytocin signaling for maternal behavior, PVN oxytocin neurons also release glutamate (Jameson et al., 2014; Chini et al., 2017; Ryan et al., 2017), and it has remained challenging to accurately detect oxytocin release within target brain areas in vivo. We therefore decided to test if pup calls can induce oxytocin release in the VTA of dams.

We first confirmed that PVN oxytocin neurons in dams project to the VTA. We injected AAV5-hSynapsin1-FLEx-axon-GCaMP6s in the PVN of Oxytocin:Cre dams, and as expected, we observed GCaMP6s+ axons in the VTA (**Figure 7A**). We then asked if pup calls trigger oxytocin release in dam VTA by using a novel genetically-encoded oxytocin sensor, *OXTR-iTango2* (Mignocchi et al., 2020). This optogenetic system allows for detection of local endogenous oxytocin release, by utilizing viral expression of oxytocin receptors and then optically labeling those neurons after oxytocin receptor signaling (**Figure 7B**). Specifically, the *OXTR-iTango2* system requires two synthetic proteins, and their interaction causes the restoration of split TEV protease function. Labelling neuronal populations with *OXTR-iTango2* consists of injecting three viral constructs in an area of interest: AAV1-hSYN-OXTR-TEV-C-P2A-iLiD-tTA (coding for the C-terminus truncated form of the oxytocin receptor, the N-terminus of TEV protease, a blue light-

sensitive protein AsLOV2, and tetracycline transactivator protein, tTA), AAV1-hSYN-β-Arrestin2-TEV-N-P2A-TdTomato (coding for β-arrestin2 protein fused with the C-terminus of the split TEV protease and tdTomato), and AAV1-hSYN-TRE-EGFP (coding for tetracycline response element, TRE, and EGFP). The reconstitution of the N- and C-termini of the TEV protease function is ligand-dependent and occurs when oxytocin binds to the oxytocin receptor. Furthermore, TEV cleavage site recognition requires presence of blue light. Thus, for *OXTR-iTango2* labelled neuronal populations to detect endogenous oxytocin release, blue light is delivered via optical fiber inserted in the same area. In the presence of oxytocin in the tissue, paired with blue light illumination, the transactivation domain TRE can trigger EGFP expression. Detection of endogenously-released oxytocin in VTA of female and male mice during social interactions has been previously demonstrated using *OXTR-iTango2* (Mignocchi et al., 2020).

To test if pup calls can trigger VTA oxytocin release in dams, we injected wild-type dams unilaterally in the left VTA with *OXTR-iTango2* viral constructs and implanted an optical fiber at the same site (**Figure 7C**). Dams were exposed to either blue light illumination and pup calls ('Blue light + pup calls'), blue light and pure tones ('Blue light + tones'), or to blue light only ('Blue light only'). Auditory stimuli (pup calls or half-octave pure tones depending on group) were played at a 0.5 Hz repetition rate and paired with blue light illumination (5 s ON/15 s OFF, for 45 min) delivered through the optical fiber connected to a blue laser (**Figure 7D**). No auditory stimuli were presented to dams in the Blue light only group. Animals were perfused and brains sectioned 48 hours after exposure. Cells expressing *OXTR-iTango2* constructs were labelled in red (tdTomato+), confirming the efficiency of the viral expression; cells expressing the TRE-EGFP reporter signal were labelled in green (EGFP+), showing neuronal populations which responded

to endogenously-released oxytocin (**Figure 7E**). There was much more EGFP reporter signal in the VTA of the Blue light + pup calls group compared to Blue light + tones or Blue light only groups (**Figures 7F-I**). This demonstrates that the enhanced firing of PVN oxytocin neurons after pup calls can lead to central oxytocin release in downstream brain areas such as the VTA.

Discussion

Here we showed that infant vocalizations can activate hypothalamic oxytocin neurons in maternal mice, inducing oxytocin release in the VTA and enhancing maternal motivation. We describe a subcortical auditory circuit to the hypothalamus, specifically from the PIL to PVN oxytocin neurons. Our data show that this circuit disinhibits oxytocin neurons and gates oxytocin release in downstream brain areas, essentially transforming acoustic input into hormonal output important for maternal care.

Pup calls increase oxytocin neuron firing via disinhibition

Classical studies described the activity of magnocellular hypothalamic neurons of dams in the contexts of nursing and parturition. These studies suggested that oxytocin neurons exhibit bursts of high-frequency action potentials in response to suckling or during the expulsive phase of labor (Wakerley and Lincoln, 1973; Summerlee, 1981; Summerlee and Lincoln, 1981; Belin and Moos, 1986; Brown and Moos, 1997). More recently, recordings in awake female mice and rats revealed that identified oxytocin neurons display lower frequency firing during social interactions with conspecifics (Carcea et al., 2019; Tang et al., 2020). We found that oxytocin neurons in awake animals exhibited sustained increases in firing lasting for hundreds of seconds after exposure to pup calls. Prolonged periods of receptivity and firing seems to be hallmark of hypothalamic neurons as they have long integration periods (Iremonger and Bains, 2007; Branco et al., 2016). Similarly, CRH neurons in PVN also exhibit a form of ramping activation in vivo in response to a looming shadow, lasting for seconds after visual stimulus offset (Daviu et al., 2020).

Unlike neurons in classical auditory areas such as the primary auditory cortex (Liu et al., 2006; Liu and Schreiner, 2007; Cohen et al., 2011; Cohen and Mizrahi, 2015; Marlin et al., 2015; Shepard et al., 2016; Tasaka et al., 2018, 2020), oxytocin neurons did not seem to exhibit stimulus-locked responses to acoustic stimuli. Instead, the duration of sustained activity in these cells was considerably long (hundreds of seconds), due to a decrease in inhibition mediated by auditory inputs from PIL. Decreased inhibition in turn resulted from NMDAR-dependent internalization of $GABA_A$Rs via dynamin signaling. Activation of NMDARs may specifically require sustained episodes of high-frequency PIL activity, as might be evoked by repeated presentation of pup calls in contrast to less-effective brief afferent stimulation (Papouin and Oliet, 2014). Previous studies have identified cross-talk between excitatory and inhibitory synapses (Piet et al., 2003, 2004; Liu 2004; Bonfardin et al., 2010; Dorrn et al., 2010; Marlin et al., 2015; Villa et al., 2016), often mediated by NMDA receptors and downstream Ca^{2+} signaling (Wang and Stelzer, 1996; Lu et al., 2000; Huang et al., 2005; Potapenko et al., 2013; Chiu et al., 2018; Field et al., 2020). It remains unclear how activation of excitatory inputs leads to a downregulation of specific inhibitory inputs.

Our results show that pup calls can act as a natural signal for relieving synaptic inhibition and enabling the activation of oxytocin neurons in dams. Both putative and identified oxytocin cells are relatively silent in vivo, having very low spontaneous firing rates (Wakerley and Lincoln, 1973; Summerlee, 1981; Summerlee and Lincoln, 1981; Belin and Moos, 1986; Brown and Moos, 1997; Carcea et al., 2019; Tang et al., 2020). This implies that oxytocin neurons are not easily activated by spontaneous synaptic events but require strong and synchronous synaptic drive to reach action potential threshold. The hypothalamus is heavily innervated by inhibitory networks from local and extrahypothalamic sources (Decavel and van den Pol, 1990; Tasker and Dudek, 1993; Johnson et

al., 2018), and inhibition increases during lactation (Giesl and Theodosis, 1994; Popescu et al., 2019). To prevent spurious milk ejection and other consequences of elevated central oxytocin, inhibitory networks must filter incoming sensory information and limit the integration of unreliable inputs in oxytocin neurons. Hypothalamic inhibition might prevent activation of oxytocin neurons by weak synaptic inputs, and instead prioritize the integration of high-frequency activity patterns specifically evoked by pup cues. Our results demonstrate how this circuit can be gated for subsequent oxytocin release in response to pup-related signals.

Central oxytocin release and maternal behavior

It has long been difficult to assess patterns and levels of central oxytocin release in vivo. Here we used a newly-developed genetically-encoded oxytocin sensor *OXTR-iTango2* (Mignocchi et al., 2020), and found that pup calls (but not pure tones) induced oxytocin release in the VTA, a region important for maternal motivation and pup retrieval behavior (Fang et al., 2018; Kohl and Dulac, 2018; Numan, 2006; Numan and Young, 2016; Rincón-Cortés and Grace, 2020). This also indicates that the firing rates of oxytocin neurons that we measured in response to pup calls were likely sufficient for release of oxytocin, as indicated by recent studies (Tang et al., 2020). Whereas higher firing frequencies of oxytocin cells might be required for peripheral muscle contraction during labor and milk ejection during nursing, lower frequency continuous firing patterns might be more appropriate for regulating complex social behaviors (Althammer and Grinevich, 2017; Dölen, 2015; Grinevich et al., 2016; Carcea et al., 2019; Tang et al., 2020; Zhang et al., 2020; Froemke and Young, 2021).

Central oxytocin signaling regulates reproduction and maternal behavior (Valtcheva and Froemke, 2019). Our findings provide a biological basis for previous reports in human mothers of increased hypothalamic activity and oxytocin release in response to baby cries (McNeilly et al., 1983; Lorberbaum et al., 2002; Swain et al., 2014; Bornstein et al., 2017). Oxytocin release throughout the central nervous system might then promote plasticity relevant for childcare and other social behaviors, depending on the context and cues linked to oxytocin neuron firing. Specifically, in the mouse auditory cortex, some cells are intrinsically tuned to certain acoustic features of baby cries (Schiavo et al., 2020). These cells might provide an upstream signal driving midbrain and then PIL activity, leading to the sustained increase in oxytocin neuron firing reported here. Oxytocin release would rapidly promote plasticity in the auditory cortex and elsewhere in the brain (Marlin et al., 2015; Froemke and Young, 2021), amplifying and elaborating neural representations across a broader range of infant cues important for parental care.

Methods

KEY RESOURCES TABLE

REAGENT or RESOURCE	SOURCE	IDENTIFIER
Antibodies		
GFP Tag Polyclonal Antibody	Thermo Fisher Scientific	A10262
Anti-mCherry antibody	Abcam	ab167453
Anti-Oxytocin Antibody	Millipore Sigma	AB911
Goat anti-Rabbit IgG (H+L) Cross-Adsorbed Secondary Antibody, Alexa Fluor 555	Thermo Fisher Scientific	A-21428
Goat anti-Chicken IgY (H+L) Secondary Antibody, Alexa Fluor 488	Thermo Fisher Scientific	A-11039
c-Fos Polyclonal rabbit purified antibody	Synaptic Systems	226 003
Bacterial and Virus Strains		
AAV1-hSyn-hChR2(H134R)-EYFP	Addgene	26973-AAV1
AAV2-EF1a-FLEX-TVA-GFP	Salk Institute Viral Vector Core	26197
AAVrg-ENN.AAV.hSyn.Cre.WPRE.hGH	Addgene	105553-AAVrg
AAV8-hSyn-DIO-hM4D(Gi)-mCherry	Addgene	44362-AAV8
AAV8-hSyn-DIO-mCherry	Addgene	50459-AAV8
EnvA G-Deleted Rabies-mCherry (SADΔG-mCherry)	Salk Institute Viral Vector Core	32636
AAV5-hSynapsin1-FLEx-axon-GCaMP6s	Addgene	112010-AAV5
AAV-DJ.CAG.Flex.GCaMP6s.WPRE.SV40	Penn Vector Core	Lot# V7340S

AAV1-hSYN-OXTR-TEV-C-P2A-iLiD-tTA	HB. Kwon	N/A
AAV1-hSYN-β-Arrestin2-TEV-N-P2A-TdTomato	Addgene	89873
AAV1-hSYN-TRE-EGFP	Addgene	89875
Chemicals, Peptides, and Recombinant Proteins		
Tissue-Plus™ O.C.T. Compound	Thermo Fisher Scientific	23-730
Triton X-100	Millipore Sigma	11332481001
Hoechst 33342	Thermo Fisher Scientific	H3570
Clozapine N-oxide hydrochloride (CNO)	Millipore Sigma	SML2304
Fluoromount-G	SouthernBiotech	0100-01
1,1'-Dioctadecyl-3,3,3',3'-Tetramethylindocarbocyanine Perchlorate (Dil Stain)	Thermo Fisher Scientific	D282
Goat Serum Donor Herd	Millipore Sigma	G6767
QX-314	Millipore Sigma	L5783
Picrotoxin	Millipore Sigma	P1675
(d(CH_2)$_5^1$,Tyr(Me)^2,Thr^4,Orn^8,des-Gly-NH_2^9)-Vasotocin trifluoroacetate salt (OTA)	Bachem	4031339
(S)-2-Amino-2-methyl-4-phosphonobutanoic acid (MAP4)	Tocris	0711
DL-2-amino-5-phosphono-pentanoic acid (AP5)	Tocris	0105
Dizocilpine maleate (MK801)	Tocris	0924
Dynamin inhibitory peptide, sequence QVPSRPNRAP	Tocris	1774
Experimental Models: Organisms/Strains		

C57BL/6N (Wild type)	Taconic	B6-F
B6;129S-*Oxt*$^{tm1.1(cre)Dolsn}$/J (oxytocin-IRES-Cre)	The Jackson Laboratory	024234
B6.Cg-*Gt(ROSA)26Sor*$^{tm32(CAG-COP4*H134R/EYFP)Hze}$/J (Ai32)	The Jackson Laboratory	024109
B6.Cg-*Gt(ROSA)26Sor*$^{tm9(CAG-tdTomato)Hze}$/J (Ai9)	The Jackson Laboratory	007909
Software and Algorithms		
Clampfit 10.7	Molecular Devices	https://www.moleculardevices.com/products/axon-patch-clamp-system/acquisition-and-analysis-software/pclamp-software-suite
Synapse	Tucker-Davis Technologies	https://www.tdt.com/component/synapse-software/
MATLAB 2017b	MathWorks	https://www.mathworks.com/products/matlab.html
Prism 9	Graphpad	https://www.graphpad.com/scientific-software/prism/

ImageJ	NIH	https://imagej.nih.gov/ij/
Adobe Audition	Adobe	https://www.adobe.com/products/audition.html
Other		
Nanoject III	Drummond Scientific	3-000-207
Pump 11 Elite Syringe Pump	Harvard Apparatus	HA1100
Hamilton syringe - 5 µL, Model 75 RN SYR	Hamilton Company	7634-01
Universal 4-Channel LED Controller	Mightex	SLC-AA02-US
Stimulus Isolator	World Precision Instruments	A365
P-97 micropipette puller	Sutter Instruments	P-97
P-100 micropipette puller	Sutter Instruments	P-100
Trough filament 3.0 mm	Sutter Instruments	FT330B
Borosilicate glass capillaries with O.D. 1.5 mm, I.D. 0.86 mm	Sutter Instruments	BF-150-86-10
Borosilicate theta capillary glass O.D. 1.5 mm, I.D. 1.00 mm	Warner instruments	TG150-4
Fiberoptic Light Stimulating Device with 465nm blue LED	A-M Systems	726500
Fiber Optic Light guide	A-M Systems	726527
Continuous Optopatcher for Current Axon Patch Clamps, AXU, 1.5 mm O.D.	A-M Systems	663943

Fiber Optic Cannula, Ø1.25 x 10.5 mm Ceramic Ferrule, Ø200 µm Core, 0.39 NA, L=5 mm	Thorlabs	CFMXB05
Fiber Optic Cannula, Ø2.5 mm Ceramic Ferrule, Ø400 µm Core, 0.50 NA, L=5 mm	Thorlabs	CFMC54L05
DPSS Blue 473 nm Laser	Opto Engine	MBL-F-473
405 nm LED	Thorlabs	M405FP1
470 nm LED	Thorlabs	M470F1
Femtowatt silicone photoreceiver	Newport	2151
LED Driver	Thorlabs	LEDD1B
Zooming lens	Thorlabs	SM1NR05
Manometer	Omega	HHP680
Tungsten Microelectrodes	Microprobes for Life Science	WE30030.5A5
DAM50 Extracellular Amplifier	World Precision Instruments	SYS-DAM50
Axopatch 200B	Molecular Devices	https://www.moleculardevices.com/products/axon-patch-clamp-system/amplifiers/axon-instruments-patch-clamp-amplifiers

Multiclamp 700B	Molecular Devices	https://www.moleculardevices.com/products/axon-patch-clamp-system/amplifiers/axon-instruments-patch-clamp-amplifiers
Digidata 1440A	Molecular Devices	https://www.moleculardevices.com/products/axon-patch-clamp-system#Digitizers
RZ6 auditory processor	Tucker-Davis Technologies	https://www.tdt.com/component/rz6-multi-i-o-processor/
RX8 Multi-I/O Processor	Tucker-Davis Technologies	https://www.tdt.com/component/rx8-multi-i-o-processor/
UltraSoundGate 116H recording interface	Avisoft-Bioacoustics	41163
Ultrasound microphone CM16/CMPA	Avisoft-Bioacoustics	40011
Custom-made 3D printed headpost and headfixation frame	This paper	N/A

LEAD CONTACT AND MATERIALS AVAILABILITY

- Further information about resources, reagents used, and requests for code should be directed to and will be fulfilled by the Lead Contacts, Silvana Valtcheva (silvana.valtcheva@uk-koeln.de) and Robert C. Froemke (robert.froemke@med.nyu.edu).
- This study did not generate new unique reagents.

EXPERIMENTAL MODEL AND SUBJECT DETAILS

Animals

All procedures were approved under NYU School of Medicine IACUC protocols, in accordance with NIH guidelines. Animals were housed in fully-equipped facilities in the NYU School of Medicine Science Building (New York City). The facilities were operated by the NYU Division of Comparative Medicine. All experimental mice were dams which had given birth for the first or second time and were housed with their own or foster pups, or were just weaned. Wild-type C57BL/6N (Taconic) dams were used for in vivo and in vitro electrophysiology, anatomy tracings, c-fos staining, oxytocin sensor experiments and behavior. Oxytocin:Cre dams were used for anatomy tracings and fiber photometry. Oxytocin:Cre x Ai9 dams were used for in vitro electrophysiology and anatomy tracings. Oxytocin:Cre x Ai32 dams were used for in vivo electrophysiology and histology validation. Mice were maintained on a normal 12-h light/dark cycle (dark cycle starts at 6 PM) and given food and water ad libitum. In vivo electrophysiology and behavioral experiments were performed at the end of the light cycle of the animals.

METHOD DETAILS

Stereotaxic surgery

Dams were anesthetized with isoflurane (1–1.5%) and bilaterally injected with 400 nL (in PVN) of either AAV2-EF1a-FLEX-TVA-GFP (Salk Institute Viral Vector Core, Item# 26197, titer: 2.73 × 10^10 vg/mL), EnvA G-Deleted Rabies-mCherry (Salk Institute Viral Vector Core, Item# 32636, titer: 3.78 × 10^7 vg/mL), AAVrg-ENN.AAV.hSyn.Cre.WPRE.hGH (Addgene, Item# 105553-AAVrg, titer: 7 × 10^12 vg/mL) or AAV5-hSynapsin1-FLEx-axon-GCaMP6s (Addgene, Item# 112010-AAV5, titer: ≥ 7 × 10^12 vg/mL) or AAVDJ-CAG-FLEx- GCaMP6s (Penn Vector Core,

Lot# V7340S, titer 3.2 × 10^13); 200 nL (in PIL) of either AAV8-hSyn-DIO-hM4D(Gi)-mCherry (Addgene, Item# 44362-AAV8, titer: 1 × 10^13 vg/mL) or AAV8-hSyn-DIO-mCherry (Addgene, Item# 50459-AAV8, titer: 1 × 10^13 vg/m); 200 nL (in PIL), 600 nL (in AuCx) or 1 µL (in IC) of AAV1-hSyn-hChR2(H134R)-EYFP (Addgene, Item# 26973-AAV1, titer: 1 × 10^13 vg/mL); unilaterally injected in the left hemisphere with 500 nL (in VTA) of *OXTR-iTango2* viral constructs of 1:1:2 ratio: AAV1-hSYN-OXTR-TEV-C-P2A-iLiD-tTA (titer: 2.1 × 10^13 vg/mL), AAV1-hSYN-β-Arrestin2-TEV-N-P2A-TdTomato (titer: 2.57 × 10^14 vg/mL), and AAV1-hSYN-TRE-EGFP (titer: 1.17 × 10^13 vg/mL). Nanoject III (Drummond Scientific, Item# 3-000-207) was used for AuCx, PIL, PVN and VTA injections. Pump 11 Elite Syringe Pump (Harvard Apparatus, Item# HA1100) with a 5 µL Hamilton syringe Model 75 RN SYR (Hamilton Company, Item# 7634-01) was used for IC injections. We waited two weeks after injection of AAV2-EF1a-FLEX-TVA-GFP to inject EnvA G-Deleted Rabies-mCherry in PVN. AAVrg-ENN.AAV.hSyn.Cre.WPRE.hGH (in PVN) and AAV8-hSyn-DIO-hM4D(Gi)-mCherry or AAV8-hSyn-DIO-mCherry (in PIL) were simultaneously injected. We used the following stereotaxic coordinates (in mm): AuCx (-2.54 A-P, +/-4.5 M-L, -0.5 D-V), IC (-5.2 A-P, +/-1.5 M-L, -1.5 D-V), PIL (-2.7 A-P, -1.7 M-L, -3.7 D-V), PVN (-0.72 A-P, +/-0.12 M-L, -4.7 D-V) and VTA (-2.5 A-P, +/-0.4 M-L, -4 D-V).

In vivo awake cell-attached and tungsten recordings

Oxytocin:Cre x Ai32 or wild-type dams were head-fixed using custom-made 3D-printed headposts and head-fixation frames. A small craniotomy (<1 mm) was performed over the sagittal sinus centered above the left PVN (coordinates in mm: -0.72 A-P, -0.12 M-L) in Oxytocin:Cre x Ai32 dams and above the left PIL (coordinates in mm: -2.7 A-P, -1.7 M-L) in wild-type dams. Cell-

attached or whole-cell recordings from optically-identified channelrhodopsin2-expressing oxytocin neurons or other unidentified neurons were obtained from the PVN (4-5.2 mm below the pial surface). Cell-attached recordings using a conventional microelectrode holder or multiunit recordings with tungsten microelectrodes of PIL neurons in wild-type dams were obtained at 3.2-3.7 mm below the pial surface. Pipettes with resistance of 5-6 MΩ and a long taper (~6 mm) designed for subcortical recordings were made of borosilicate glass capillaries with O.D. 1.5 mm, I.D. 0.86 mm (Sutter Instruments, Item# BF-150-86-10) using P-87 micropipette puller (Sutter Instruments, Item# P-87) and a 3 mm trough filament (Sutter Instruments, Item# FT330B). Patch pipettes contained (in mM): 127 K-gluconate, 8 KCl, 10 phosphocreatine, 10 HEPES, 4 Mg-ATP, 0.3 Na-GTP (osmolality, 285 mOsm; pH 7.2 adjusted with KOH). The pressure of the patch pipette was monitored with manometer (Omega, Item# HHP680). 15-20 mbar pressure was applied when the patch pipette was lowered into the brain and the pressure was adjusted to 1.5-2 mbar when the pipette reached the targeted depth from the pial surface. Cell-attached recordings were obtained with a Multiclamp 700B amplifier (Molecular Devices) and data were acquired with Clampex 10.7 (Molecular Devices), low-pass filtered at 1 kHz, high-pass filtered at 100 Hz and digitized at 20 kHz. Multiunit recordings were obtained using tungsten microelectrodes (Microprobes for Life Science, Item# WE30030.5A5) with 2-3 μm diameter and 0.5 MΩ impedance connected to DAM50 Extracellular Amplifier (World Precision Instruments); data were acquired with Clampex 10.7 (Molecular Devices), low-pass filtered at 3 kHz, high-pass filtered at 300 Hz and digitized at 100 kHz. The tip of the tungsten electrode was coated with DiI for histological validation of the recording site.

In vivo optogenetic identification of PVN neurons

To identify channelrhodopsin2-expressing PVN oxytocin neurons in Oxytocin:Cre x Ai32 dams via channelrhodopsin2-assisted patching during each recording session (Katz et al., 2013; Muñoz et al., 2014, 2017), we used a Fiberoptic Light Stimulating Device with 465nm blue LED (A-M Systems, Item# 726500) connected to a Fiber Optic Light guide (A-M Systems, Item# 726527). The optic fiber was inserted into the patch pipette via 1.5 mm O.D. Continuous Optopatcher holder (A-M Systems, Item# 663943). Pulses of blue light were delivered through the optic fiber via Digidata 1440A (Molecular Devices) while recording in cell-attached or whole-cell configuration the responses of channelrhodopsin2-positive oxytocin neurons (ChR2+; OT+) or other channelrhodopsin2-negative PVN neurons (ChR2-; OT-). Different steps of light pulses (50 or 200 ms duration) were delivered with increasing intensity from 20 to 100% of full LED power (3 mW at the tip of the fiber). ChR2+ (OT+) neurons responded to light pulses by an increase in their firing rate and spiking probability, while ChR2- (OT-) neurons were not modulated by blue light.

Fiber photometry

Oxytocin:Cre dams were bilaterally injected with AAVDJ-CAG-FLEx- GCaMP6s (Penn Vector Core, Lot# V7340S, titer 3.2 × 10^13) in PVN (coordinates in mm: -0.72 A-P, +/-0.12 M-L, -4.7 D-V). Animals were head-posted and a 400 µm optical fiber (Thorlabs, Item# CFMC54L05) was implanted in the left hemisphere slightly above the injection site at -4.5 D-V. Experiments were performed two to three weeks after surgery. Dams were placed in a head-fixation frame within a custom-built soundproof box and photometry was performed with a custom-built rig (Falkner et al., 2016; Carcea et al., 2019). A 400 Hz sinusoidal blue light (40-45 µW) from a 470 nm LED (Thorlabs, Item# M470F1) connected to a LED driver (Thorlabs, Item# LEDD1B) was delivered

via the optical fiber to excite GCaMP6s. We also used a control 330 Hz light (10 μW) from a 405 nm LED (Thorlabs, Item# M405FP1) connected to a second LED driver. Light travelled via 405 nm and 469 nm excitation filters via a dichroic mirror to the brain. Emitted light traveled back through the same optical fiber via dichroic mirror and 525 nm emission filter, passed through an adjustable zooming lens (Thorlabs, Item# SM1NR05) and was detected by a femtowatt silicon photoreceiver (Newport, Item# 2151). Recordings were performed using RX8 Multi-I/O Processor (Tucker-Davis Technologies). The envelopes of the signals were extracted in real time using Synapse software (Tucker-Davis Technologies). The analog readout was low-pass filtered at 10 Hz.

Auditory stimulation

Pup distress vocalizations were recorded from isolated pups aged postnatal day (P) 2-8 using an ultrasonic microphone (CM16/CMPA, Avisoft Bioacoustics, Item# 41163, 200 kHz sampling rate; connected to UltraSoundGate 116H recording interface, Avisoft-Bioacoustics, Item# 41163) and de-noised/matched in peak amplitude (Adobe Audition) similar to previous work (Schiavo et al., 2020). To investigate responses to pup calls in individual oxytocin neurons, we monitored baseline firing rates for 1-2 min. For most cells, we then played a set of pup calls (RZ6 auditory processor, Tucker-Davis Technologies) consisting of 3-5 individual pup calls (~1 s duration of each call) repeated for a total of 15-18 calls with a 1 sec delay between calls. Most calls were isolation/distress calls; for one neuron, wriggling calls were played. For the cells in **Figure S2D-F**, individual calls were played after 1 s baselines, with 3-6 different pup calls were played for 10-15 times each. For the fiber photometry experiments (**Figure 2**), we played 5 sets of pup calls separated by 1-3 minutes each. For studies of pure tones (**Figures S2G-I, S3G and H**), half-octave

pure tones ranging 4–64 kHz (50 ms, 10 ms cosine ramp) at 70 dB sound pressure level (SPL) were played using RZ6 auditory processor (Tucker-Davis Technologies) in a pseudorandom order (repetition rate: 0.2 Hz).

In vitro whole-cell recordings

Recordings in brain slices were conducted two to three weeks after virus injection. After being anesthetized by isoflurane inhalation, mice were perfused with ice-cold sucrose-based cutting solution containing (in mM): 87 NaCl, 75 sucrose, 2.5 KCl, 1.25 NaH2PO4, 0.5 CaCl2, 7 MgCl2, 25 NaHCO3, 1.3 ascorbic acid, and 10 D-Glucose, bubbled with 95%/5% O_2/CO_2 (pH 7.4). The brain was rapidly placed in the same solution and slices were prepared with a vibratome (Leica P-1000), placed in warm artificial cerebrospinal fluid (ACSF, in mM: 124 NaCl, 2.5 KCl, 1.5 MgSO4, 1.25 NaH2PO4, 2.5 CaCl2, and 26 NaHCO3), bubbled with 95%/5% O_2/CO_2 (pH 7.4), and maintained at 33-35°C for <30 min, then cooled to room temperature (22-24°C) for at least 40 min before use. For experiments, slices were transferred to the recording chamber and superfused (2.5-3 $ml.min^{-1}$) with ACSF at 33°C bubbled with 95%/5% O_2/CO_2 (pH 7.4). PVN oxytocin neurons (red fluorescent) or PIL neurons (non-fluorescent) were identified with an Olympus 40 x water-immersion objective with TRITC filter. Pipettes with resistance 5-6 MΩ made of borosilicate glass capillaries with O.D. 1.5 mm, I.D. 0.86 mm (Sutter, Item# BF-150-86-10) contained for voltage-clamp recordings (in mM): 130 Cs-methanesulfonate, 1 QX-314, 4 TEA-Cl, 0.5 EGTA, 10 phosphocreatine, 10 HEPES, 4 Mg-ATP, 0.3 Na-GTP (osmolality, 285 mOsm; pH 7.32 adjusted with CsOH), or for current-clamp recordings (in mM): 127 K-gluconate, 8 KCl, 10 phosphocreatine, 10 HEPES, 4 Mg-ATP, 0.3 Na-GTP (osmolality, 285 mOsm; pH 7.2 adjusted with KOH). Somatic whole-cell voltage-clamp and current-clamp recordings were made from

PVN oxytocin neurons or PIL neurons with an Multiclamp 200B amplifier (Molecular Devices). Data were acquired with Clampex 10.7 (Molecular Devices), low-pass filtered at 2 kHz and digitized at 20 kHz. To measure synaptic connectivity between areas using channelrhodopsin2-assisted circuit mapping (Petreanu et al., 2007), whole-cell voltage-clamp recordings were made and neurons were held at -70 mV for EPSC recordings. Channelrhodopsin2-expressing axons were activated with 1 ms pulses of full field illumination with 465 nm LED light (Mightex, Item# SLC-AA02-US) repeated at 0.1 Hz. To measure NMDAR-mediated currents, whole-cell voltage-clamp recordings were made in the presence of picrotoxin [50 μM] and neurons were held at +40 mV. Amplitudes of NMDAR-mediated currents was measured 50 ms after optogenetic stimulation.

Long-term synaptic plasticity experiments

Whole-cell current-clamp or voltage-clamp recordings were made from PVN oxytocin neurons (red fluorescent) of Oxytocin:Cre x Ai9 dams injected with AAV1-hSyn-hChR2(H134R)-EYFP in PIL. Action potentials or synaptic currents were evoked using an extracellular bipolar electrode made of 0.015" silver-chloride filament inserted into a borosilicate theta capillary glass O.D. 1.5 mm, I.D. 1.00 mm (Warner Instruments, Item# TG150-4) filled with ACSF and placed lateral and in close proximity to PVN. To evoke a single action potential or postsynaptic potentials in current-clamp mode, or synaptic currents in voltage-clamp mode, electrical pulses (0.1-10 mA and 0.1 ms duration) were delivered at 0.1 Hz with Stimulus Isolator (World Precision Instruments, Item# A365). To examine action potential generation, baselines were recorded for 2.5 min (15 sweeps) and the intensity of the electrical stimulation was tuned to remain mainly subthreshold. Optogenetic stimulation of PIL terminals in PVN (PIL opto; 30 Hz during 1 s, repeated at 0.5 Hz for 3 min) was designed to mimic PIL discharge during pup call presentation in vivo; subthreshold

activity or evoked action potentials were recorded for 20 min (120 sweeps) after PIL opto. For monitoring synaptic currents, neurons were held at -70 mV for EPSCs and 0 mV for IPSCs. Neurons were held at -50 mV during PIL opto. Following PIL opto, synaptic currents were recorded for 15-20 min. For excitability experiments, neurons were recorded in current-clamp configuration and held at ~-50 mV (close to resting membrane potential). Number of evoked spikes by different amplitudes of intracellular current injection was calculated before and after PIL opto. Recordings were excluded from analysis if the access resistance (Ra) changed >30% compared to baseline. (d$(CH_2)_5^1$,Tyr(Me)^2,Thr^4,Orn^8,des-Gly-NH_2^9)-Vasotocin trifluoroacetate salt (OTA; 1 µM; Bachem, Item# 4031339), DL-2-amino-5-phosphono-pentanoic acid (AP5; 50 µM; Tocris, Item# 0105), (S)-2-Amino-2-methyl-4-phosphonobutanoic acid (MAP4; 250 µM; Tocris, Item# 0711) and clozapine N-oxide hydrochloride (CNO; 1 µM; Millipore Sigma, Item# SML2304) were dissolved directly in the extracellular solution and bath applied. Picrotoxin (50 µM; Millipore Sigma, Item# P1675) was dissolved in ethanol and added to the extracellular solution, such that the final concentration of ethanol was 0.1%. Dizocilpine maleate (MK801; 1 mM; Tocris, Item# 0924) and Dynamin inhibitory peptide, sequence QVPSRPNRAP (1.5 mM; Tocris, Item# 1774) were dissolved directly in the intracellular solution.

c-fos labelling

Dams were allowed to habituate for 15 min with an ultrasound speaker present in their home cage. Experiments were performed in the absence of pups in the cage. A set of pup calls consisting of 6 different calls was presented at 0.5 Hz repetition rate (~1 s duration of each call and 1 sec delay between calls) for a total of 10 min. After the end of the pup call playback, dams were left in their

home cage (no pups present) for 60-90 min before being anesthetized and perfused for histology as described below.

Chemogenetic inactivation

Wild-type dams were bilaterally injected with AAVrg-ENN.AAV.hSyn.Cre.WPRE.hGH in PVN and with either AAV8-hSyn-DIO-hM4D(Gi)-mCherry or AAV8-hSyn-DIO-mCherry in PIL. Pup retrieval behavior was measured three weeks after virus injection. 1-2 days before behavior testing, dams were housed in a 26 x 34 x 18 cm cage with pups of P1-5 and nesting material. The day of behavior testing, dams were intraperitoneally injected with 1 mg/kg clozapine N-oxide hydrochloride (CNO) or the equivalent volume of saline and pup retrieval behavior was measured. Two to four pups were left in the nest and the remaining pups were kept away from the cage and used for retrieval testing. After verifying that the dam was in the nest, one pup was placed in the corner of the cage opposite to the nest. The dam was given ten trials (2 min per trial) to retrieve the displaced pup and return it back to the nest; if the displaced pup was not retrieved within 2 min, the pup was removed and the trial was scored as a failure. Another pup was then placed in an opposite corner and the next trial begun. If dams retrieved pups with 90% accuracy under saline conditions, they were injected with CNO and pup retrieval behavior was tested again after 30-40 min. Behavioral performance (time to retrieval and success rate) for each dam was compared between saline and CNO conditions. Each session of testing consisted of a baseline set (under saline injection) of 10 trials and a post-CNO injection set of 10 trials. Experiments were performed under red light.

Oxytocin sensor

Wild-type dams were unilaterally injected in the left hemisphere with *OXTR-iTango2* viral constructs (1:1:2 ratio; AAV1-hSYN-OXTR-TEV-C-P2A-iLiD-tTA, AAV1-hSYN-β-Arrestin2-TEV-N-P2A-TdTomato, and AAV1-hSYN-TRE-EGFP) in VTA (coordinates in mm: -2.5 A-P, -0.4 M-L, -4 D-V). A 200 µm optical fiber (Thorlabs, Item# CFMXB05) was also implanted in the VTA using the same coordinates and a head-post was installed. Pup calls, pure tones, and blue light exposure was performed three weeks after surgery. Dams were head-fixed during experiments. Animals in Blue light + pup calls group were exposed to pup calls (5 different pup calls; ~1 s duration; 0.5 Hz repetition rate; RZ6 auditory processor, Tucker-Davis Technologies) and paired with blue light illumination (5 s ON/15 s OFF; DPSS Blue 473 nm laser, Opto Engine, Item# MBL-F-473) for 45 min. Animals in Blue light + tones group were exposed to half-octave pure tones (ranging 4–64 kHz; 1 s duration, 10 ms cosine ramp, 70 dB SPL, 0.2 Hz repetition rate) played in a pseudorandom order with blue light illumination (5 s ON/15 s OFF) for 45 min. Animals in Blue light only group were exposed to blue light illumination only (5 s ON/15 s OFF) for 45 min.

Histology and imaging

Animals were deeply anaesthetized with isoflurane inhalation followed by intraperitoneal injection (0.1 ml per 10 g) of a ketamine–xylazine mixture containing 15 mg/ml ketamine and 5 mg/ml xylazine, and transcardially perfused with phosphate buffered saline (PBS) followed by 4% paraformaldehyde (PFA) in PBS. Brains were immersed overnight in 4% PFA followed by immersion in 30% sucrose for two nights. Brains were embedded with Tissue-Plus™ O.C.T. Compound medium (Thermo Fisher Scientific, Item# 23-730) and sectioned at 50 µm thickness

using a cryostat (Leica). After cryosectioning, brain sections were washed with PBS (3 x 10 min at room temperature) in a staining jar and incubated for 2 h at room temperature in blocking solution containing 5% normal goat serum (Millipore Sigma, Item# G6767) in 1% Triton X-100 (Millipore Sigma, Item# 11332481001) dissolved in PBS, followed by 48 h incubation at room temperature with primary antibodies at 1:500 dilution in 3% normal goat serum in 1% Triton X-100 dissolved in PBS. Sections were washed with PBS (3 x 10 min at room temperature) and incubated for 2 h at room temperature in Alexa-Fluor-conjugated secondary antibodies diluted at 1:500 in PBS. Following washing with PBS (2 x 10 min at room temperature), sections were incubated with Hoechst 33342 (Thermo Fisher Scientific, Item# H3570) at 1:1000 for nuclear staining. After washing with PBS (2 x 10 min at room temperature), slides were coverslipped using Fluoromount-G (SouthernBiotech). Slides were examined and imaged using a Carl Zeiss LSM 700 confocal microscope with four solid-state lasers (405/444, 488, 555, 639 nm) and appropriate filter sets.

QUANTIFICATION AND STATISTICAL ANALYSIS

Electrophysiology

Off-line analysis was performed with Clampfit 10.7 (Molecular Devices). Spikes were automatically detected by threshold crossing. To investigate long-term responses to pup calls, normalized firing rate was computed by calculating percentage change in firing rate each minute. To investigate responses to individual pup calls, firing rate was measured throughout the call duration plus 300-400 ms, compared to spontaneous firing 1 s before call onset. To investigate responses to pure tones, firing rate was measured 100 ms from onset of the tone compared to spontaneous rate 100 ms before tone onset. Z-scores were computed by calculating the call-evoked

firing rate relative to the spontaneous firing rate: $z = (\mu_{evoked} - \mu_{spontaneous}) / \sigma_{spontaneous}$ (Marlin et al., 2015).

Fiber photometry

Data from both the 470 (signal) and 405 (control) wavelength channels were independently filtered using a sliding window (Bruno et al., 2020). The scale of the control channel was normalized using a least-squares regression of the 470 and 405 wavelength channels. $\Delta F/F$ was generated by subtracting the normalized control channel from the signal channel. For analysis including all animals, 'Pre' was the 20 seconds prior to pup call onset, 'Calls' was the period of call playback, and 'Post' was 40 seconds after call offset.

Oxytocin sensor

The *OXTR-iTango2* labeled population in the VTA was categorized into four types based on red and green fluorescent signals from *post hoc* confocal imaging data analysis. Individual regions of interest (ROIs) for cells were semi-automatically drawn using a custom algorithm (ImageJ) based on fluorescence intensity, cell size, and cell shape. The average red (R) and green (G) fluorescent signals were calculated for each ROI and were divided by the mean background value (R_0 and G_0 for red and green channels, respectively) outside of the ROIs for normalization. ROIs were allocated into four different quadrants divided by thresholds in two fluorescent colors (x-axis: red tdTomato signal, red threshold value: -1.5; y-axis: green EGFP TRE reporter signal, green threshold value: 0.585). ROIs with red signals above or below the red threshold value were categorized as tdTomato+ or tdTomato-, respectively. ROIs with green signals above or below the green threshold value were categorized as EGFP+ or EGFP-, respectively.

Statistics

Electrophysiology data analysis was performed using Clampfit (Molecular Devices). Fiber photometry analysis was performed using MATLAB 2017b (MathWorks). Image analysis was conducted using NIH ImageJ. In experiments with paired samples, we used Wilcoxon matched-pairs signed rank two-tailed test (**Figures 4J, 5A, 6D, 6F, 6G, S1F, S2C, S2E, S3E, S5D, S5E, S5F and S5G**) or Friedman test (**Figure 1H**). One-sample two-tailed Student's t-test was used in **Figures 1J, 4D, 4F, 4G, 5C, 5E, 5G, 6E, S3F, S4E, S6B, S6D, S6E, S6F, S6G and S6H**. Mann-Whitney two-tailed test was used in **Figures 4C, 4E, 5B, 5D, 5F, 5I, 6F, S1G, S6A and S6C**. One-way ANOVA was used in **Figures 2F, 7I, S1B, S1D, S1E and S2F**. All sample sizes and definitions as well precision measures (mean, SEM or SD) are provided in figure legends. Statistical tests and graph generation were performed using Prism 9 (GraphPad) or MATLAB 2017b (MathWorks).

DATA AND CODE AVAILABILITY

All data and code are available upon request.

Figure 1. Pup calls activate PVN oxytocin neurons in vivo.

(**A**) Schematic of experimental design: in vivo cell-attached and whole-cell channelrhodopsin2-assisted recordings in PVN of awake head-fixed Oxytocin:Cre x Ai32 dams, pup calls playback via ultrasonic speaker. PVN, paraventricular nucleus of the hypothalamus.

(**B**) Image of PVN of Oxytocin:Cre x Ai32 dams showing that neurons expressing EYFP-ChR2 also expressed oxytocin peptide. Scale, 100 µm (inset, 10 µm). 3V, third ventricle.

(**C**) In vivo optogenetic identification of PVN neurons: ChR2+ (OT+) neurons exhibited reliable spiking responses to pulses of blue light ('Opto'), ChR2- (OT-) neurons did not.

(**D**) Location (depth from pia) and firing rate of cell-attached (n=19 neurons from N=8 dams) and whole-cell (n=1 from N=1) recordings of ChR2+ OT+ neurons and ChR2- neurons (OT-, cell-attached: n=16, N=8; whole-cell: n=2, N=2).

(**E, F**) Example traces from cell-attached recordings of ChR2+ (OT+) neuron and ChR2- (OT-) neuron showing baseline spiking activity preceding onset of pup calls (1, 'Pre', upper trace), activity during playback of a set of pup calls ('Calls', middle trace) and activity at 80 sec after the onset of pup calls playback (2, 'Post', lower trace). Firing rates during baseline and after pup calls were calculated over 1-2 min. The set of pup calls consisted of 15-18 calls with 1 s silence gap in between. Inset: each pink bar represents a single pup call. Note increased firing rate for ChR2+ (OT+) neuron but not ChR2- (OT-) neuron following pup calls playback.

(**G**) Peristimulus time histograms for example ChR2+ (OT+) and ChR2- (OT-) neurons from **E, F**. Bins: 10 s.

(**H**) Firing rate during baseline ('Pre'), pup call playback ('Calls'), and after pup calls ('Post', peak firing rate over 20-60 s) of ChR2+ (OT+, left; Pre: 2.9±0.7 Hz, Post: 5.0±1.6 Hz, n=12, N=6;

p=0.001, Friedman test) and ChR2- (OT-, right; Pre: 3.1±0.9 Hz, Post: 3.6±1.0 Hz, n=11, N=5; p=0.07) neurons.

(**I**) Post-call sustained increase in firing rates of ChR2+ (OT+, left; n=12, N=6) but not ChR2- (OT-, right; n=11, N=5) neurons.

(**J**) Change in firing rate of ChR2+ (OT+; 227±42.8% of baseline; cell-attached: n=11, N=6; whole-cell: n=1, N=1; p=0.01, one-sample two-tailed Student's t-test) neurons but not ChR2- (OT-; 121.8±12.7% of baseline; cell-attached: n=9, N=5; whole-cell: n=2, N=2; p=0.12) neurons. Cell-attached (circles) and whole-cell (triangles) recordings.

Data reported as mean±SEM. *p<0.05, **p<0.01.

See also Figures S1 and S2.

Figure 2. Population activity of PVN oxytocin neurons in vivo in response to pup calls.

(**A**) Left, schematic showing injection of AAVDJ-CAG-FLEx-GCaMP6s in the PVN of Oxytocin:Cre dams and optical fiber implantation. Right, histological confirmation of GCaMP6s expression and fiber implantation. Scale, 200 μm. PVN, paraventricular nucleus of the hypothalamus; 3V, third ventricle.

(**B**) Schematic of experimental design: fiber photometry recordings in PVN of awake head-fixed Oxytocin:Cre dams and pup calls playback from an ultrasonic speaker.

(**C-F**) Oxytocin neurons responded to pup calls. (**C**) Example trace showing changes in GCaMP6s fluorescence following playback of one set of pup calls ('Calls'; 15 pup calls, 1 second gap in between calls). (**D**) Timeline of responses to five sets of pup calls ('Calls'; x15 calls each) in one example animal. (**E, F**) Z-scores of fluorescence activity preceding onset of pup calls (1, 'Pre') and following pup calls playback (2, 'Post') for example animal (**E**) and summary (**E, F**; Post: 2.3±3.8, N=4, p=0.016, one-way ANOVA).

Data reported as mean±SEM. *p<0.05.

Figure 3. PVN oxytocin neurons receive projections from PIL.

(**A-E**) Cell-type specific rabies virus tracing of monosynaptic auditory inputs onto PVN oxytocin neurons. (**A**) Injection of helper virus construct AAV2-EF1a-FLEX-TVA-GFP followed by injection of the *Cre*-inducible, retrograde pseudotyped monosynaptic rabies virus SADΔG-mCherry two weeks later in PVN of Oxytocin:Cre dams. (**B**) Validation of injection site showing starter oxytocin neurons in PVN expressing TVA-GFP and ΔG-RV-mCherry. Scale, 100 µm. (**C-E**) Retrograde rabies infection and mCherry staining was absent in MGB (**C**), AuCx (**D**), and IC (**E**). Dense rabies-infected field and robust expression of mCherry was found in PIL (**C**; N=4 dams). Scale, 500 µm. AuCx, auditory cortex; IC, inferior colliculus; MGB, medial geniculate body of the thalamus; PIL, posterior intralaminar nucleus of the thalamus; PVN, paraventricular nucleus of the hypothalamus; SN, substantia nigra; 3V, third ventricle.

(**F, G**) PIL receives reliable input from IC. (**F**; left) Injection of AAV1-hSyn-hChR2(H134R)-EYFP in IC of wild-type dams followed by whole-cell voltage-clamp recordings from PIL neurons in vitro. (Right) Validation of injection site in IC showing ChR2-EYFP expression and IC projections in MGB and PIL. Scale, 200 µm. (**G**) Mean amplitude and latency of optogenetically-induced EPSCs (oEPSCs) in PIL neurons in response to optogenetic stimulation (vertical blue line) of IC axons in acute slices of PIL. Synaptic connections found in 10/12 neurons from N=5 dams.

(**H, I**) PIL receives sparser input from AuCx. (**H**; left) Injection of AAV1-hSyn-hChR2(H134R)-EYFP in AuCx of wild-type dams followed by whole-cell voltage-clamp recordings from PIL neurons in vitro. (Right) Validation of injection site in AuCx showing ChR2-EYFP expression and dense AuCx projections in MGB but sparser in PIL. Scales, 500 µm and 200 µm, respectively. (**I**) Mean amplitude and latency of oEPSCs in PIL neurons in response to optogenetic stimulation of AuCx axons in acute slices of PIL. Synaptic connections found in 4/13 neurons from N=3 dams.

(**J, K**) PVN oxytocin neurons receive reliable input from PIL. (**J**) Injection of AAV1-hSyn-hChR2(H134R)-EYFP in PIL of Oxytocin:Cre x Ai9 dams followed by whole-cell voltage-clamp recordings from oxytocin neurons (tdTomato+) in vitro. (**J**; left) Validation of injection site in PIL showing ChR2-EYFP expression and PIL projections in PVN. Scales, 200 µm and 100 µm, respectively. (**K**) Mean amplitude and latency of oEPSCs in oxytocin neurons in response to optogenetic stimulation of PIL axons in acute slices of PVN. Synaptic connections found in 49/62 neurons from N=23 dams.

Data reported as mean±SEM.

See also Figure S3.

Figure 4. Enhanced spiking of PVN oxytocin neurons via iLTD following optogenetic activation of PIL inputs.

(**A**) Schematic showing injection of AAV1-hSyn-hChR2(H134R)-EYFP in PIL of Oxytocin:Cre x Ai9 dams 2-3 weeks prior to whole-cell recordings from oxytocin neurons (tdTomato+) in PVN brain slices. PIL, posterior intralaminar nucleus of the thalamus; PVN, paraventricular nucleus of the hypothalamus.

(**B**) Schematic showing whole-cell recordings from tdTomato+ oxytocin neurons in acute slice of PVN, as well as optogenetic stimulation of PIL axons ('PIL opto') and the placement of the extracellular stimulation electrode.

(**C-G**) PIL opto induced iLTD in oxytocin neurons. Whole-cell voltage-clamp recordings showed no change in EPSC magnitude after PIL opto; example cell (**C**; p=0.15, Mann-Whitney two-tailed test; scale, 20 ms and 50 pA) and summary (**D**; n=7 neurons, p=0.14, one-sample two-tailed Student's t-test). Whole-cell voltage-clamp recordings showed decreased IPSC magnitudes after PIL opto; example cell (**E**; p<0.0001, Mann-Whitney; scale, 20 ms and 100 pA) and summary (**F**; n=10, p=0.0003, one-sample Student's t-test). (**G**) IPSC/EPSC ratio decreased following PIL opto (p=0.0018, one-sample Student's t-test).

(**H-J**) Long-term increase in spiking probability of oxytocin neurons following PIL opto. (**H**) Example trace from whole-cell current-clamp recording showing improved spiking output of oxytocin neuron following PIL opto. (**I**) Timeline of long-term spiking probability in response to PIL opto (n=6). (**J**) Spiking probability was significantly increased at 20 min after PIL opto (n=6, p=0.03, Wilcoxon matched-pairs signed rank two-tailed test).

Data reported as mean±SEM (**J**) or as mean±SD (**D, F, G and I**). *p<0.05, **p<0.01.

See also Figures S4 and S5.

Figure 5. iLTD in oxytocin neurons relies on postsynaptic NMDARs and dynamin signaling.

(**A**) Optogenetic stimulation of PIL (vertical blue line) triggered NMDAR-dependent currents in oxytocin neurons which were blocked by bath-application of AP5 (50 μM; n=7 neurons, p=0.02, Wilcoxon matched-pairs signed rank two-tailed test).

(**B, C**) iLTD in oxytocin neurons is NMDAR-dependent. Whole-cell voltage-clamp recordings showing no plasticity after optogenetic stimulation of PIL terminals in PVN ('PIL opto') in presence of bath-applied AP5 (50 μM), for example neuron (**B**; p=0.62, Mann-Whitney two-tailed test) and summary (**C**; n=8, p=0.44, one-sample two-tailed Student's t-test).

(**D, E**) iLTD in oxytocin neurons is dependent on postsynaptic NMDARs. Whole-cell voltage-clamp recordings showing no plasticity after PIL opto when i-MK801 (1 mM) was applied in the recording pipette, for example neuron (**D**; p=0.11, Mann-Whitney) and summary (**E**; n=6, p=0.18, one-sample Student's t-test).

(**F, G**) iLTD in oxytocin neurons is dependent on dynamin signaling. Whole-cell voltage-clamp recordings showing no plasticity after PIL opto when i-Dynamin inhibitor (1.5 mM) was applied in the recording pipette, for example neuron (**F**; p=0.30, Mann-Whitney) and summary (**G**; n=7, p=0.63, one-sample Student's t-test).

(**H**) Schematic of the PVN synapse showing possible mechanisms for postsynaptic NMDAR-dependent decrease in inhibition. OXTR, oxytocin receptor.

(**I**) iLTD is blocked by AP5 (p=0.0021, Mann-Whitney), i-MK801 (p=0.02) and i-Dynamin inhibitor (p=0.0068) but not by MAP4 (p=0.37) or OTA (p=0.08).

Data reported as mean±SEM (**A and I**) or as mean±SD (**C, E and G**). *p<0.05, **p<0.01, ns: not significant.

See also Figure S6.

Figure 6. Chemogenetic inhibition of PIL projections to PVN slows down pup retrieval behavior.

(**A**) Experimental schematic showing injection of AAVrg-ENN.AAV.hSyn.Cre.WPRE.hGH in PVN and AAV8-hSyn-DIO-hM4D(Gi)-mCherry or AAV8-hSyn-DIO-mCherry in PIL of wild-type dams.

(**B**) Histology validation of mCherry expression in PVN-projecting PIL neurons. Scale, 200 µm. MGB, medial geniculate body of the thalamus; PIL, posterior intralaminar nucleus of the thalamus; SN, substantia nigra.

(**C-E**) Bath-application of CNO (1 µM) reduced firing rate in PIL brain slices from dams expressing hM4Di. Example whole-cell current-clamp recording from PIL neuron (**C**) showing a significant decrease in spiking in the presence of CNO (**D**; n=6 neurons, p=0.03, Wilcoxon matched-pairs signed rank two-tailed test; **E**; p=0.003, one-sample two-tailed Student's t-test).

(**F**) Dams expressing hM4Di and injected with CNO had longer pup retrieval latencies compared to saline controls (hM4Di: CNO vs saline, N=11, p=0.01, Wilcoxon) and dams expressing mCherry (mCherry: CNO vs saline, N=6, p=0.16, Wilcoxon; across groups for saline hM4Di vs mCherry, p=0.15, Mann-Whitney two-tailed test; for CNO hM4Di vs mCherry, p=0.02, Mann-Whitney).

(**G**) No difference in pup retrieval probability between dams expressing either hM4Di (CNO vs saline, N=11, p=0.47, Wilcoxon) or mCherry (CNO vs saline, N=6, p>0.99).

Data reported as mean±SEM. *p<0.05.

Figure 7. Pup calls trigger oxytocin release in the VTA.

(**A**) Injection of AAV5-hSynapsin1-FLEx-axon-GCaMP6s in the PVN of Oxytocin:Cre dams (left). GCaMP6s+ axons were found in the VTA (right). Scale, 200 μm. N=2 dams. PVN, paraventricular nucleus of the hypothalamus; VTA, ventral tegmental area.

(**B**) Schematic of *OXTR-iTango2* genetic strategy.

(**C**) Injection of *OXTR-iTango2* viral constructs (AAV1-hSYN-OXTR-TEV-C-P2A-iLiD-tTA, AAV1-hSYN-β-Arrestin2-TEV-N-P2A-TdTomato, and AAV1-hSYN-TRE-EGFP) and optical fiber implantation in VTA.

(**D**) Headfixed dams were exposed to either pup calls paired with blue light delivered through the optical fiber connected to a blue laser (Blue light + pup calls group), pure tones paired with blue light (Blue light + tones), or blue light alone (Blue light only).

(**E**) Example image of VTA neurons expressing *OXTR-iTango2* constructs with TRE-EGFP reporter in the Blue light + pup calls group (left; scale, 200 μm) and magnified images from the area marked by a square (right; scale, 50 μm).

(**F-H**) Distribution patterns of gene expression and percentage of *OXTR-iTango2* labeled neurons VTA of dams. Neuronal populations shown in example confocal images were divided into four quadrants (black dashed lines indicate the threshold for dividing each quadrant): cells with no viral infection (tdTomato-/EGFP-; black, 'B'); cells with only TRE-reporter signal (tdTomato-/EGFP+; green, 'G'), cells with only β-Arrestin-tdTomato signal (tdTomato+/EGFP-; red, 'R'); cells with both red and green signal (tdTomato+/EGFP+; yellow, 'Y'). Scatter plots allocate individual cells into the four different quadrants by red (x-axis: tdTomato, R/R_0) and green (y-axis: EGFP, G/G_0) fluorescent colors. Blue light + pup calls ('BL+PC'; N=5; **F**), Blue light + tones ('BL+T'; N=4; **G**), and Blue light only ('BL'; N=5; **H**). Scale, 50 μm.

(**I**) Density quantification of *OXTR-iTango2* labeled cells. There was a significant amount of yellow (tdTomato+/EGFP+) cells in the Blue light + pup calls ('BL+PC') compared to Blue light + tones ('BL+T') group ($p<0.0001$, one-way ANOVA; $p<0.0001$ with *post hoc* Bonferroni correction) or Blue light only group ('BL'; $p=0.0002$). There was no difference in the amount of yellow cells between Blue light + pure tones and Blue light only groups ($p=0.78$).

Data reported as mean±SEM. **$p<0.01$, ns: not significant.

Figure S1. Identification of ChR2+ (OT+) and ChR2- (OT-) neurons. Related to Figure 1.

(**A**) Sample traces and raster plots of cell-attached recordings from one ChR2+ (OT+, left) and one ChR2- (OT-, right) neuron showing reliable activation of ChR2+ (OT+) neurons in response to 50 ms pulses of blue light at 5 Hz (20-100% laser power).

(**B**) Increase in the number of spikes (left) of ChR2+ (OT+; pink circles; n=7 neurons, N=5 dams, $p<0.0001$, one-way ANOVA) and spike probability (right; $p<0.0001$) in response to 50 ms light pulse steps. Number of spikes of ChR2- (OT-; black circles; n=13, N=3, p=0.07) neurons, as well as spike probability (p=0.11) was not modulated.

(**C**) Sample traces and raster plots of cell-attached recordings of one ChR2+ (OT+, left) and one ChR2- (OT-, right). ChR2+ (OT+) neuron was reliably activated in response to 200 ms pulses of blue light (0-100% laser power).

(**D**) Increase in the number of spikes (left) of ChR2+ (OT+; pink circles; n=9, N=6, $p<0.0001$, one-way ANOVA) and spike probability (right; $p<0.0001$) in response to 200 ms light pulse steps. Number of spikes of ChR2- (OT-; black circles; n=13, N=3, p=0.61) neurons, as well as spike probability (p=0.73) was not modulated.

(**E**) Increase in firing rate of ChR2+ (OT+; n=10, N=5, p=0.0001, one-way ANOVA) but not of ChR2- (OT-; n=13, N=3, p=0.68) neurons in response to 200 ms light pulse of 100% laser power ('Opto') compared to their baseline firing rate immediately preceding ('Pre') and immediately after ('Post') the light pulse.

(**F**) Change of firing rate of ChR2+ (OT+; n=10, N=5, p=0.002, Wilcoxon matched-pairs signed rank two-tailed test) but not of ChR2- (OT-; n=13, N=3, p=0.91) neurons in response to 200 ms light pulse of 100% laser power ('Opto') compared to baseline firing immediately preceding the light pulse ('Pre').

(**G**) Latency to first spike was significantly shorter in ChR2+ (OT+; n=14, N=6, $p<0.0001$, Mann-Whitney two-tailed test) compared to ChR2- (OT-; n=8, N=2) neurons in response to 200 ms light pulse of 100% laser power. 'First spike' in ChR2- (OT-) cells was not light-evoked but occurred spontaneously.

Data reported as mean±SEM. **, $p<0.01$.

Figure S2. In vivo responses to individual pup calls and pure tones. Related to Figure 1.

(**A, B**) Sample traces of whole-cell recordings of one ChR2+ (OT+; **A**) and one ChR2- (OT-; **B**) neuron showing baseline spiking activity preceding onset of pup calls ('Pre', upper trace), activity during playback of a set of pup calls ('Calls', middle trace) and activity after pup calls playback ('Post', lower trace). Note increased firing rate for ChR2+ (OT+) neuron but not ChR2- (OT-) neuron.

(**C**) ChR2+ (OT+) did not respond to individual pup calls within a set. 'Pre', average spiking rate of cell-attached recordings during all baseline periods immediately preceding each call within the set. 'Call', average spiking rate during pup call stimulus for each call within the set. Neither ChR2+ (OT+; n=9 neurons, N=6 dams, p=0.38, Wilcoxon matched-pairs signed rank two-tailed test), nor ChR2- (OT-; n=9, N=5, p=0.30) neurons increased their firing rate during individual calls ('Call') compared to baseline ('Pre').

(**D-F**) ChR2+ (OT+) did not respond to repetitive presentation of individual pup calls on a trial-by-trial basis. (**D**) Sample traces of cell-attached recordings of one ChR2+ (OT+), one ChR2- (OT-) and one unidentified PVN neuron, as well as whole-cell recording of a PVN neuron during trial-by-trial individual pup call presentation. (**E**) No increase in the firing rates of either ChR2+ (OT+; n=8, N=2, p=0.38, Wilcoxon), ChR2- (OT-; n=7, N=3, p=0.08), or unidentified PVN (cell-attached: n=26, N=13; whole-cell: n=6, N=4, p=0.48) neurons during individual pup calls ('Call') compared to baseline ('Pre') on a trial-by-trial basis. (**F**) No difference in the z-scores of spiking responses of cell-attached and whole-cell recordings during individual pup calls in ChR2+ (OT+; n=8, N=2, p=0.30, one-way ANOVA), ChR2- (OT-; n=7, N=4), and unidentified PVN (cell-attached: n=26, N=13; whole-cell: n=6, N=4) neurons.

(**G-I**) PVN neurons did not respond to pure tones. Example cell-attached recording of one PVN neuron in response to 23 kHz tone presentation (**G**) and tuning profile of pure tone frequency responses in this cell (**H**). (**I**) Average tuning profile of pure tone frequency responses in PVN cells (n=15, N=9).

Data reported as mean±SEM.

Figure S3. Auditory projections to PVN. Related to Figure 3.

(**A, B**) Expression of c-fos in MGB and PIL of dams after playback of pup calls. Scale, 200 µm. N=3. MGB, medial geniculate body of the thalamus; PIL, posterior intralaminar nucleus of the thalamus; SN, substantia nigra.

(**C-F**) In vivo activation of PIL during playback of pup calls. (**C**; left) Experimental setup showing in vivo multiunit recordings via tungsten electrode in PIL of awake head-fixed wild-type dams while playing pup calls from an ultrasound speaker. (**C**; right) Validation of PIL recording site by coating tungsten electrode tip with DiI. Scale, 500 µm. (**D-F**) Increase of multiunit spiking activity in PIL during playback of pup calls in vivo (**E**; N=6 dams, p=0.03, Wilcoxon matched-pairs signed rank two-tailed test) which corresponded to a significant increase from baseline values (**F**; p=0.02, one-sample two-tailed Student's t-test).

(**G-H**) PIL exhibits responses to pure tones. Example of multiunit spiking activity recorded with tungsten electrode in PIL in response to 23 kHz tone presentation (**G**) and tuning profile of pure tone frequency responses in PIL (**H**; N=5).

(**I**) PVN does not receive input from IC. Left, injection of AAV1-hSyn-hChR2(H134R)-EYFP in IC of wild-type dams. Right, no EYFP staining was found in PVN, suggesting that IC does not project to PVN. Scale, 200 µm. N=3. IC, inferior colliculus; PVN, paraventricular nucleus of the hypothalamus.

(**J**) PVN does not receive input from AuCx. Left, injection of AAV1-hSyn-hChR2(H134R)-EYFP in AuCx of wild-type dams. Right, no EYFP staining was found in PVN, suggesting that AuCx does not project to PVN. Scale, 200 µm. N=2. AuCx, auditory cortex.

Data reported as mean±SEM. *p<0.05.

Figure S4. PIL neurons do not exhibit sustained increase in baseline firing rate following pup calls in vivo. Related to Figure 4.

(**A**) Experimental setup showing in vivo cell-attached recordings in PIL of awake wild-type dams while playing pup calls from an ultrasound speaker. PIL, posterior intralaminar nucleus of the thalamus.

(**B**) Location (depth from pia) and firing rate of PIL neurons (n=9 neurons; N=4 dams).

(**C-E**) PIL neurons did not modulate their firing rate following playback of a set of pup calls (15 pup calls, 1 second gap in between calls). (**C**) Sample traces from a cell-attached recording of one PIL neuron showing its baseline firing rate immediately preceding (1, 'Pre') and at 90 sec after the onset of pup calls playback (2, 'Post'). Firing rates during baseline and after pup calls were calculated over 1-2 min. (**D, E**) PIL neurons did not exhibit persistent increase in baseline firing following pup calls, as calculated between 80-160 sec after onset of pup call playback (**E**, n=9, N=4, p=0.77, one-sample two-tailed Student's t-test).

Data reported as mean±SEM. ns: not significant.

Figure S5. PIL opto does not affect the excitability of oxytocin neurons. Related to Figure 4.

(**A**) Schematic showing injection of AAV1-hSyn-hChR2(H134R)-EYFP in PIL of Oxytocin:Cre x Ai9 dams 2-3 weeks prior to whole-cell recordings from oxytocin neurons (tdTomato+) in PVN brain slices. PIL, posterior intralaminar nucleus of the thalamus; PVN, paraventricular nucleus of the hypothalamus.

(**B**) Schematic showing whole-cell recordings from tdTomato+ oxytocin neurons in acute slice of PVN, as well as optogenetic stimulation of PIL axons ('PIL opto').

(**C, D**) No change in the number of spikes in oxytocin neurons in response to 20 pA steps of intracellular current injection before ('Pre') or after ('Post') PIL opto. Sample traces (**C**) and summary (**D**; n=9 neurons, p>0.44, Wilcoxon matched-pairs signed rank two-tailed test).

(**E-G**) No change in the intrinsic properties of oxytocin neurons after PIL opto, in terms of rheobase (**E**; n=9; p=0.38, Wilcoxon), resting membrane potential (**F**; n=6; p=0.16), or input resistance (**G**; n=12; p=0.06).

Data reported as mean±SEM.

Figure S6. iLTD in oxytocin neurons is not dependent on type-III mGluRs or oxytocin signaling. Related to Figure 5.

(**A, B**) Whole-cell voltage-clamp recordings showing intact iLTD after optogenetic stimulation of PIL terminals in PVN ('PIL opto') in presence of bath-applied type-III mGluR antagonist MAP4 (250 μM), for example neuron (**A**; $p<0.0001$, Mann-Whitney two-tailed test; axis: 20 ms, 50 pA) and summary (**B**; n=5 neurons, p=0.02, one-sample two-tailed Student's t-test).

(**C, D**) Whole-cell voltage-clamp recordings showing intact iLTD after PIL opto in presence of bath-applied OXTR antagonist OTA (1 μM), for example neuron (**C**; $p<0.0001$, Mann-Whitney; axis: 20 ms, 50 pA) and summary (**D**; n=8, p=0.0009, one-sample Student's t-test).

(**E-G**) Timecourse of unchanged IPSC/EPSC ratio in the presence of AP5 (**E**; p=0.07, one-sample Student's t-test), i-MK801 (**F**; p=0.68), or i-Dynamin inhibitor (**G**; p=0.91).

(**H**) IPSC/EPSC ratio was not changed after PIL opto in presence of AP5 (p=0.07, one-sample Student's t-test), i-MK801 (p=0.68), or i-Dynamin inhibitor (p=0.91), but was significantly decreased in control conditions (p=0.0018), and in the presence of OTA (p=0.0003).

Data reported as mean±SEM (**H**) or mean±SD (**B**, **D**, **E**, **F** and **G**). *$p<0.05$, **$p<0.01$, ns: not significant.

References

Althammer, F., and Grinevich, V. (2017). Diversity of oxytocin neurones: Beyond magno- and parvocellular cell types? J Neuroendocr. Online ahead of print.

Bannai, H., Niwa, F., Mark, W., Triller, A., Le, S., Bannai, H., Niwa, F., Sherwood, M.W., Shrivastava, A.N., and Arizono, M. (2015). Bidirectional control of synaptic GABAAR clustering by glutamate and calcium. Cell Rep. 13, 2768–2780.

Belin, V., and Moos, F. (1986). Paired recordings from supraoptic and paraventricular oxytocin cells in suckled rats: recruitment and synchronization. J. Physiol. 377, 369–90.

Bonfardin, V.D.J., Fossat, P., Theodosis, D.T., and Oliet, S.H.R. (2010). Glia-dependent switch of kainate receptor presynaptic action. J. Neurosci. 30, 985–995.

Bordi, F., and LeDoux, J.E. (1994a). Response properties of single units in areas of rat auditory thalamus that project to the amygdala: I. Acoustic discharge patterns and frequency receptive fields. Exp Brain Res 98, 261–274.

Bordi, F., and LeDoux, J.E. (1994b). Response properties of single units in areas of rat auditory thalamus that project to the amygdala: II. Cells receiving convergent auditory and somatosensory inputs and cells antidromically activated by amygdala stimulation. Exp Brain Res 98, 275–286.

Bornstein, M.H., Putnick, D.L., Rigo, P., Esposito, G., Swain, J.E., Suwalsky, J.T.D., Su, X., Du, X., Zhang, K., Cote, L.R., De Pisapia, N., and Venuti, P. (2017). Neurobiology of culturally common maternal responses to infant cry. Proc. Natl. Acad. Sci. 114, E9465–E9473.

Boudaba, C., Szabo, K., and Tasker, J.G. (1996). Physiological mapping of local inhibitory inputs to the hypothalamic paraventricular nucleus. J Neurosci 16, 7151–7160.

Bourque, C.W., and Renaud, L.P. (1991). Membrane properties of rat magnocellular neuroendocrine cells in vivo. Brain Res. 540, 349–352.

Branco, T., Tozer, A., Christopher, J., Lee, A.K., Wood, J.N., and Sternson, S.M. (2016). Near-perfect synaptic integration by Nav1.7 in hypothalamic neurons regulates body weight. Cell 165, 1749–1761.

Brown, C.H., Bains, J.S., Ludwig, M., and Stern, J.E. (2013). Physiological regulation of magnocellular neurosecretory cell activity: Integration of intrinsic, local and afferent mechanisms. Neuroendocrinology. J Neuroendocrinol. 678–710.

Brown, C.H., Ludwig, M., Tasker, J.G., and Stern, J.E. (2020). Somato-dendritic vasopressin and oxytocin secretion in endocrine and autonomic regulation. J Neuroendocr. 32, e12856.

Brown, D., and Moos, F. (1997). Onset of bursting in oxytocin cells in suckled rats. J. Physiol. 503, 625–634.

Bruno, C.A., O'Brien, C., Bryant, S., Mejaes, J., Pizzano, C., Estrin, D.J., and Barker, D.J. (2020). pMAT: An open-source, modular software suite for the analysis of fiber photometry calcium imaging. bioRxiv.

Brussaard, A.B., Kits, K.S., and Vlieger, T.A. de (1996). Postsynaptic mechanism of depression of GABAergic synapses by oxytocin in the supraoptic nucleus of immature rat. J Physiol 497, 495–507.

Cai, D., Yue, Y., Su, X., Liu, M., Wang, Y., You, L., Xie, F., Deng, F., Chen, F., Luo, M., and Yuan, K. (2018). Distinct anatomical connectivity patterns differentiate subdivisions of the nonlemniscal auditory thalamus in mice. Cereb. Cortex 29, 2437-2454.

Campeau, S., and Watson, S.J. (2000). Connections of some auditory-responsive posterior thalamic nuclei putatively involved in activation of the hypothalamo-pituitary-adrenocortical axis in response to audiogenic stress in rats : An anterograde and retrograde tract tracing study combined. J. Comp. Neurol. 491, 474–491.

Carcea, I., Caraballo, N.L., Marlin, B.J., Ooyama, R., Riceberg, J.S., Navarro, J.M.M., Opendak, M., Diaz, V.E., Schuster, L., Torres, M.I.A., Lethin, H., Ramos, D., Minder, J., Mendoza, S.L., Hidema, S., Falkner, A., Lin, D., Mar, A., Wadghiri, Y.Z., Nishimori, K., Kikusui, T., Mogi, K., Sullivan, R.M., and Froemke, R.C. (2019). Oxytocin neurons enable social transmission of maternal behavior. bioRxiv.

Chini, B., Verhage, M., and Grinevich, V. (2017). The action radius of oxytocin release in the mammalian CNS: From single vesicles to behavior. Trends Pharmacol. Sci. 11, 982-991.

Chiu, C.Q., Martenson, J.S., Yamazaki, M., Tomita, S., Tavalin, S.J., and Higley, M.J. (2018). Input-specific NMDAR-dependent potentiation of dendritic GABAergic inhibition. Neuron 97, 368-377.

Cohen, L., Rothschild, G., and Mizrahi, A. (2011). Multisensory integration of natural odors and sounds in the auditory cortex. Neuron 72, 357–369.

Cohen, L., and Mizrahi, A. (2015). Plasticity during motherhood: Changes in excitatory and inhibitory Layer 2 / 3 neurons in auditory cortex. J Neurosci 35, 1806–1815.

Cservenák, M., Bodnár, I., Usdin, T.B., Palkovits, M., Nagy, G.M., and Dobolyi, A. (2010). Tuberoinfundibular peptide of 39 residues is activated during lactation and participates in the suckling-induced prolactin release in rat. Neuroendocrinology 151, 5830–5840.

Cservenák, M., Szabo, E.R., and Usdin, T.B. (2013). Thalamic neuropeptide mediating the effects of nursing on lactation and maternal motivation. Psychoneuroendocrinology 38, 3070–3084.

Cservenák, M., Keller, D., Kis, V., Fazekas, E.A., Öllös, H., Lékó, A.H., Szabó, E.R., Renner, E., Usdin, T.B., Palkovits, M., and Dobolyi, A. (2017). A thalamo-hypothalamic pathway that activates oxytocin neurons in social contexts in female rats. Endocrinology 158, 335–348.

Daviu, N., Füzesi, T., Rosenegger, D.G., Rasiah, N.P., Sterley, T., Peringod, G., and Bains, J.S. (2020). Paraventricular nucleus CRH neurons encode stress controllability and regulate defensive behavior selection. Nat. Neurosci. 23, 398–410.

de Kock, C.P.J., Wierda, K.D.B., Bosman, L.W.J., Min, R., Koksma, J., Mansvelder, H.D., Verhage, M., and Brussaard, A.B. (2003). Somatodendritic secretion in oxytocin neurons is upregulated during the female reproductive cycle. J Neurosci 23, 2726–2734.

de Kock, C.P.J., Burnashev, N., Lodder, J.C., Mansvelder, H.D., and Brussaard, A.B. (2004). NMDA receptors induce somatodendritic secretion in hypothalamic neurones of lactating female rats. J. Physiol. 561, 53–64.

Decavel, C., and van den Pol, A. (1990). GABA: A dominant neurotransmitter in the hypothalamus. J Comp Neurol 1037, 1019–1037.

Dobolyi, A., Palkovits, M., Bodnár, I., and Usdin, T.B. (2003). Neurons containing tuberoinfundibular peptide of 39 residues project to limbic, endocrine, auditory and spinal areas in rat. Neuroscience 122, 1093–1105.

Dobolyi, A., Cservenák, M., and Young, L.J. (2018). Thalamic integration of social stimuli regulating parental behavior and the oxytocin system. Front. Neuroendocrinol. 51, 102–115.

Dölen, G. (2015). Oxytocin: Parallel processing in the social brain? J. Neuroendocrinol. 27, 516–535.

Dorrn, A.L., Yuan, K., Barker, A.J., Schreiner, C.E., and Froemke, R.C. (2010). Developmental sensory experience balances cortical excitation and inhibition. Nature 465, 932–936.

Dulac, C., O'Connell, L., and Wu, Z. (2014). Neural control of maternal and paternal behaviors. Science 345, 1063–1069.

Ehret, G. (2005). Infant rodent ultrasounds - A gate to the understanding of sound communication. Behav. Genet. 35, 19–29.

Esposito, G., Manian, N., Truzzi, A., and Bornstein, M.H. (2017). Response to infant cry in clinically depressed and non-depressed mothers. PLoS One 12, 1–15.

Factor, E.M., Mayer, A.D., and Rosenblatt, J.S. (1993). Peripeduncular nucleus lesions in the rat: I. Effects on maternal aggression, lactation, and maternal behavior during pre- and postpartum periods. Behav Neurosci 107, 166–185.

Falkner, A.L., Grosenick, L., Davidson, T.J., Deisseroth, K., and Lin, D. (2016). Hypothalamic control of male aggression-seeking behavior. Nat. Neurosci. 19, 596-604.

Fang, Y.-Y., Yamaguchi, T., Song, S.C., Tritsch, N.X., and Lin, D. (2018). A hypothalamic midbrain pathway essential for driving maternal behaviors. Neuron 98, 192-207.e10.

Feldman, R. (2016). The neurobiology of human attachments. Trends Cogn. Sci. 21, 80–99.

Field, R.E., James, A.D., Tremblay, R., Miehl, C., Rudy, B., Gjorgjieva, J., and Froemke, R.C. (2020). Heterosynaptic plasticity determines the set point for cortical excitatory-inhibitory balance. Neuron 5, 842-854.

Fleming, T.M., Scott, V., Naskar, K., Joe, N., Brown, C.H., and Stern, J.E. (2011). State-dependent changes in astrocyte regulation of extrasynaptic NMDA receptor signalling in neurosecretory neurons. J. Physiol. 589, 3929–3941.

Freund-Mercier, M.J., Moos, F., Poulain, D.A., Richard, P., Rodriguez, F., Theodosis, D.T., Vincent, J.-D. (1988). Role of central oxytocin in the control of the milk ejection reflex. Brain Res. Bull. 20, 737–741.

Froemke, R.C., and Young, L.J. (2021), Oxytocin, neural plasticity, and social behavior, Annu Rev Neurosci, in press

Giesl, U., and Theodosis, T. (1994). Synaptic plasticity in the rat supraoptic nucleus during lactation involves GABA innervation and oxytocin neurons : A quantitative immunocytochemical analysis. J Neurosci 14, 2861-2869.

Grinevich, V., Knobloch-Bollmann, H.S., Eliava, M., Busnelli, M., and Chini, B. (2016). Assembling the puzzle: Pathways of oxytocin signaling in the brain. Biol. Psychiatry 79, 155–164.

Grinevich, V., Stoop, R., 2018. Interplay between oxytocin and sensory systems in the orchestration of socio-emotional behaviors. Neuron 99, 887–904.

Hansen, S., Harthon, C., Wallin, E., Löfberg, L., and Svensson, K. (1991). Mesotelencephalic dopamine system and reproductive behavior in the female rat: Effects of ventral tegmental 6-hydroxydopamine lesions on maternal and sexual responsiveness. Behav. Neurosci. 105, 588–598.

Hansen, S., and Köhlerb, C. (1984). The importance of the peripeduncular nucleus in the neuroendocrine control of sexual behavior and milk ejection in the rat. Neuroendocrinology 572, 563–572.

Haucke, V., Neher, E., and Sigrist, S.J. (2011). Protein scaffolds in the coupling of synaptic exocytosis and endocytosis. Nat. Neurosci. Rev. 12, 127–138.

Herring, D., Huang, R., Singh, M., Dillon, G.H., and Leidenheimer, N.J. (2005). PKC modulation of GABAA receptor endocytosis and function is inhibited by mutation of a dileucine motif within the receptor beta 2 subunit. Neuropharmacology 48, 181–194.

Huang, C.S., Shi, S.H., Ule, J., Ruggiu, M., Barker, L.A., Darnell, R.B., Jan, Y.N., and Jan, L.Y. (2005). Common molecular pathways mediate long-term potentiation of synaptic excitation and slow synaptic inhibition. Cell 123, 105–118.

Hung, L., Neuner, S., Plepalli, J., Beier, K., Wright, M., Walsh, J., Luo, L., Deisseroth, K., Dölen, G., and Malenka, R. (2017). Gating of social reward by oxytocin in the ventral tegmental area. Science 1411, 1406–1411.

Iremonger, K.J., and Bains, J.S. (2007). Integration of asynchronously released quanta prolongs the postsynaptic spike window. J. Neurosci. 27, 6684–6691.

Jameson, H., Popratiloff, A., Lee, N.H., and Mendelowitz, D. (2014). Visualization of oxytocin release that mediates paired pulse facilitation in hypothalamic pathways to brainstem autonomic neurons. PLoS One 9, 3–9.

Johnson, C.S., Bains, J.S., and Watts, A.G. (2018). Neurotransmitter diversity in pre-synaptic terminals located in the parvicellular neuroendocrine paraventricular nucleus of the rat and mouse hypothalamus. J. Comp. Neurol. 526, 1287–1306.

Jurek, B., and Neumann, I.D. (2018). The oxytocin receptor: From intracellular signaling to behavior. Physiol. Rev. 98, 1805–1908.

Katz, Y., Yizhar, O., Staiger, J., and Lampl, I. (2013). Optopatcher - An electrode holder for simultaneous intracellular patch-clamp recording and optical manipulation. J. Neurosci. Methods 214, 113–117.

Kim, S., Soeken, T.A., Cromer, S.J., Martinez, S.R., Hardy, L.R., and Strathearn, L. (2014). Oxytocin and postpartum depression: Delivering on what's known and what's not. Brain Res. 1580, 219–232.

Kohl, J., and Dulac, C. (2018). Neural control of parental behaviors. Curr. Opin. Neurobiol. 49, 116–122.

Larsen, P.J., Hay-Schmidt, A., and Mikkelsen, J.D. (1994). Efferent connections from the lateral hypothalamic region and the lateral preoptic area to the hypothalamic paraventricular nucleus of the rat. J Comp Neurol 319, 299–319.

LeDoux, J.E., Ruggiero, D.A., Forest, R., Stornetta, R., and Reis, D.J. (1987). Topographic organization of convergent projections to the thalamus from the inferior colliculus and spinal cord in the rat. J Comp Neurol 146, 123-146.

Leng, G., Brown, C.H., and Russell, J.A. (1999). Physiological pathways regulating the activity of magnocellular neurosecretory cells. Prog. Neurobiol. 57, 625–655.

Lewis, E.M., Stein-O'Brien, G.L., Patino, A. V., Nardou, R., Grossman, C.D., Brown, M., Bangamwabo, B., Ndiaye, N., Giovinazzo, D., Dardani, I., Jiang, C., Goff, L.A., and Dölen, G. (2020). Parallel social information processing circuits are differentially impacted in autism. Neuron 108, 659-675.

Linke, R., 1999. Differential projection patterns of superior and inferior collicular neurons onto posterior paralaminar nuclei of the thalamus surrounding the medial geniculate body in the rat. Eur. J. Neurosci. 11, 187–203.

Liu, G. (2004). Local structural balance and functional interaction of excitatory and inhibitory synapses in hippocampal dendrites. Nat. Neurosci. 7, 373–379.

Liu, R.C., Linden, J.F., and Schreiner, C.E. (2006). Improved cortical entrainment to infant communication calls in mothers compared with virgin mice. Eur J Neurosci 23, 3087–3097.

Liu, R.C., and Schreiner, C.E. (2007). Auditory cortical detection and discrimination correlates with communicative significance. PLoS Biol. 5, e173.

Livneh, Y., Ramesh, R.N., Burgess, C.R., Levandowski, K.M., Madara, J.C., Fenselau, H., Goldey, G.J., Diaz, V.E., Jikomes, N., Resch, J.M., Lowell, B.B., and Andermann, M.L. (2017). Homeostatic circuits selectively gate food cue responses in insular cortex. Nature 546, 611–616.

Lorberbaum, J.P., Newman, J.D., Horwitz, A.R., Dubno, J.R., Lydiard, R.B., Hamner, M.B., Bohning, D.E., and George, M.S. (2002). A potential role for thalamocingulate circuitry in human maternal behavior. Biol. Psychiatry 51, 431–445.

Lu, Y.M., Mansuy, I.M., Kandel, E.R., and Roder, J. (2000). Calcineurin-mediated LTD of GABAergic inhibition underlies the increased excitability of CA1 neurons associated with LTP. Neuron 26, 197–205.

Ludwig, M., and Leng, G. (2006). Dendritic peptide release and peptide-dependent behaviours. Nat. Rev. Neurosci. 7, 126–136.

Lyons, D.J., and Broberger, C. (2014). TIDAL WAVES: Network mechanisms in the neuroendocrine control of prolactin release. Front. Neuroendocrinol. 35, 420–438.

Marlin, B.J., Mitre, M., D'Amour, J.A., Chao, M. V, and Froemke, R.C. (2015). Oxytocin enables maternal behaviour by balancing cortical inhibition. Nature 520, 499–504.

McNeilly, A.S., Robinson, I.C., Houston, M.J., and Howie, P.W. (1983). Release of oxytocin and prolactin in response to suckling. Br. Med. J. (Clin. Res. Ed). 286, 257–259.

Mignocchi, N., Jung, K., Lee, D., and Kwon, H.-B. (2020). Development of a genetically-encoded oxytocin sensor. bioRxiv.

Mitre, M., Marlin, B.J., Schiavo, J.K., Morina, E., Norden, S.E., Hackett, T.A., Aoki, X.C.J., Chao, M. V, and Froemke, R.C. (2016). A distributed network for social cognition enriched for oxytocin receptors. J. Neurosci. 36, 2517–2535.

Muñoz, W., Tremblay, R., and Rudy, B. (2014). Channelrhodopsin-assisted patching: In vivo recording of genetically and morphologically identified neurons throughout the brain. Cell Rep. 2304–2316.

Muñoz, W., Tremblay, R., Levenstein, D., and Rudy, B. (2017). Layer-specific modulation of neocortical dendritic inhibition during active wakefulness. Science 959, 954–959.

Murakami, T.C., Mano, T., Saikawa, S., Horiguchi, S.A., Shiget, D., Baba, K., Sekiya, H., Shimizu, Y., Tanaka, K.F., and Kiyonari, H. (2018). A three-dimensional single-cell-resolution whole-brain. Nat. Neurosci. 21, 625–637.

Naskar, K., and Stern, J.E. (2014). A functional coupling between extrasynaptic NMDA receptors and A-type K+ channels under astrocyte control regulates hypothalamic neurosecretory neuronal activity. J. Physiol. 592, 2813–2827.

Neumann, I., Russell, J.A., and Landgraf, R. (1993). Oxytocin and vasopressin release within the supraoptic and paraventricular nuclei of pregnant, parturient and lactating rats: A microdialysis study. Neuroscience 53, 65–75.

Neumann, I.D., and Landgraf, R. (2012). Balance of brain oxytocin and vasopressin: Implications for anxiety, depression, and social behaviors. Trends Neurosci. 35, 649–659.

Numan, M. (2006). Hypothalamic neural circuits regulating maternal responsiveness toward infants. Behav. Cogn. Neurosci. Rev. 5, 163–190.

Numan, M., Stolzenberg, D.S., Dellevigne, A.A., Correnti, C.M., and Numan, M.J. (2009). Temporary inactivation of ventral tegmental area neurons with either muscimol or baclofen reversibly disrupts maternal behavior in rats through different underlying mechanisms. Behav. Neurosci. 123, 740–751.

Numan, M., and Young, L.J. (2016). Neural mechanisms of mother-infant bonding and pair bonding: Similarities, differences, and broader implications. Horm. Behav. 77, 98–112.

Oliet, S.H.R., Baimoukhametova, D. V., Piet, R., and Bains, J.S. (2007). Retrograde regulation of GABA transmission by the tonic release of oxytocin and endocannabinoids governs postsynaptic firing. J. Neurosci. 27, 1325–1333.

Owen, S.F., Tuncdemir, S.N., Bader, P.L., Tirko, N.N., Fishell, G., and Tsien, R.W. (2013). Oxytocin enhances hippocampal spike transmission by modulating fast-spiking interneurons. Nature 500, 458–462.

Palkovits, M., Dobolyi, A., Helfferich, F., and Usdin, T.B. (2004). Localization and chemical characterization of the audiogenic stress pathway. Ann N Y Acad Sci 24, 16–24.

Panatier, A., Poulain, D.A., and Oliet, S. (2004). Regulation of transmitter release by high-affinity group III mGluRs in the supraoptic nucleus of the rat hypothalamus. Neuropharmacology 47, 333–341.

Papouin, T., and Oliet, S.H.R. (2014). Organization, control and function of extrasynaptic NMDA receptors. Philos. Trans. R. Soc. Lond. B. Biol. Sci. 369, 20130601.

Paquet, M., and Smith, Y. (2000). Presynaptic NMDA receptor subunit immunoreactivity in GABAergic terminals in rat brain. J Comp Neurol 347, 330–347.

Pawluski, J.L., Lonstein, J.S., and Fleming, A.S. (2017). The neurobiology of postpartum anxiety and depression. Trends Neurosci. 40, 106–120.

Pedersen, C.A., Caldwell, J.D., Walker, C., Ayers, G., and Mason, G.A. (1994). Oxytocin activates the postpartum onset of rat maternal behavior in the ventral tegmental and medial preoptic areas. Behav. Neurosci. 108, 1163–1171.

Petreanu, L., Huber, D., Sobczyk, A., and Svoboda, K. (2007). Channelrhodopsin-2-assisted circuit mapping of long-range callosal projections. Nat. Neurosci. 10, 663–668.

Piet, R., Bonhomme, R., Theodosis, D.T., Poulain, D.A., and Oliet, S.H.R. (2003). Modulation of GABAergic transmission by endogenous glutamate in the rat supraoptic nucleus. Eur. J. Neurosci. 17, 1777–1785.

Piet, R., Vargová, L., Syková, E., Poulain, D.A., and Oliet, S.H.R. (2004). Physiological contribution of the astrocytic environment of neurons to intersynaptic crosstalk. Proc. Natl. Acad. Sci. U. S. A. 101, 2151–2155.

Popescu, I.R., Buraei, Z., Haam, J., Weng, F.-J., and Tasker, J.G. (2019). Lactation induces increased IPSC bursting in oxytocinergic neurons. Physiol. Rep. 7, 1–11.

Potapenko, E.S., Biancardi, V.C., Zhou, Y., and Stern, J.E. (2013). Astrocytes modulate a postsynaptic NMDA–GABAA-Receptor crosstalk in hypothalamic neurosecretory neurons. J Neurosci 33, 631–640.

Resendez, S.L., Namboodiri, V.M.K., Otis, J.M., Eckman, L.E.H., Rodriguez-romaguera, J., Ung, R.L., Basiri, X.M.L., Kosyk, O., Rossi, M.A., Dichter, G.S., and Stuber, X.G.D. (2020). Social stimuli induce activation of oxytocin neurons within the paraventricular nucleus of the hypothalamus to promote social behavior in male mice. J Neurosci 40, 2282–2295.

Rilling, J.K., and Young, L.J. (2014). The biology of mammalian parenting and its effect on offspring social development. Science 345, 771–776.

Rincón-Cortés, M., and Grace, A.A. (2020). Adaptations in reward-related behaviors and mesolimbic dopamine function during motherhood and the postpartum period. Front. Neuroendocrinol. 57, 100839.

Roland, B.L., and Sawchenko, P.E. (1993). Local origins of some GABAergic projections to the paraventricular and supraoptic nuclei of the hypothalamus in the rat. J. Comp. Neurol. 332, 123–143.

Romanov, R.A., Zeisel, A., Bakker, J., Girach, F., Hellysaz, A., Tomer, R., Alpár, A., Mulder, J., Clotman, F., Keimpema, E., Hsueh, B., Crow, A.K., Martens, H., Schwindling, C., Calvigioni, D., Bains, J.S., Máté, Z., Szabó, G., Yanagawa, Y., Zhang, M.D., Rendeiro, A., Farlik, M., Uhlén, M., Wulff, P., Bock, C., Broberger, C., Deisseroth, K., Hökfelt, T., Linnarsson, S., Horvath, T.L., and Harkany, T. (2017). Molecular interrogation of hypothalamic organization reveals distinct dopamine neuronal subtypes. Nat. Neurosci. 20, 176–188.

Ryan, P.J., Ross, S.I., Campos, C.A., Derkach, V.A., and Palmiter, R.D. (2017). Oxytocin-receptor-expressing neurons in the parabrachial nucleus regulate fluid intake. Nat. Neurosci. 20, 1722-1733.

Schiavo, J.K., Valtcheva, S., Bair-Marshall, C.J., Song, S.C., Martin, K.A., and Froemke, R.C. (2020). Innate and plastic mechanisms for maternal behaviour in auditory cortex. Nature. 587, 426-431.

Schrader, L.A., and Tasker, J.G. (1997). Presynaptic modulation by metabotropic glutamate receptors of excitatory and inhibitory synaptic inputs to hypothalamic magnocellular neurons. J Neurophysiol. 2, 527–36.

Shahrokh, D.K., Zhang, T.Y., Diorio, J., Gratton, A., and Meaney, M.J. (2010). Oxytocin-dopamine interactions mediate variations in maternal behavior in the rat. Endocrinology 151, 2276–2286.

Shepard, K.N., Chong, K.K., and Liu, R.C. (2016). Contrast enhancement without transient map expansion for species-specific vocalizations in core auditory cortex during learning. eNeuro 3, ENEURO.0318-16.2016.

Smith, P.H., Bartlett, E.L., Kowalkowski, A., Ph, S., El, B., and Cortical, K.A. (2007). Cortical and collicular inputs to cells in the rat paralaminar thalamic nuclei adjacent to the medial geniculate body. J Neurophysiol 98, 681–695.

Summerlee, A.J. (1981). Extracellular recordings from oxytocin neurones during the expulsive phase of birth in unanaesthetized rats. J. Physiol. 321, 1–9.

Summerlee, A., and Lincoln, D. (1981). Electrophysiological recordings from oxytocinergic neurones during suckling in the unanaesthetized lactating rat. J Endocrinol 90, 255–65.

Sun, L., and Liu, S.J. (2007). Activation of extrasynaptic NMDA receptors induces a PKC-dependent switch in AMPA receptor subtypes in mouse cerebellar stellate cells. J Physiol 2, 537–553.

Swain, J.E., Kim, P., Spicer, J., Ho, S.S., Dayton, C.J., Elmadih, A., and Abel, K.M. (2014). Approaching the biology of human parental attachment: Brain imaging, oxytocin and coordinated assessments of mothers and fathers. Brain Res. 1580, 78–101.

Tang, Y., Benusiglio, D., Lefevre, A., Hilfiger, L., Althammer, F., Bludau, A., Hagiwara, D., Baudon, A., Darbon, P., Schimmer, J., Kirchner, M.K., Roy, R.K., Wang, S., Eliava, M., Wagner, S., Oberhuber, M., Conzelmann, K.K., Schwarz, M., Stern, J.E., Leng, G., Neumann, I.D., Charlet, A., and Grinevich, V. (2020). Social touch promotes interfemale communication via activation of parvocellular oxytocin neurons. Nat. Neurosci. 9, 1125–1137.

Tasaka, G.I., Guenthner, C.J., Shalev, A., Gilday, O., Luo, L., and Mizrahi, A. (2018). Genetic tagging of active neurons in auditory cortex reveals maternal plasticity of coding ultrasonic vocalizations. Nat. Commun. 9, 871.

Tasaka, G., Feigin, L., Maor, I., Froemke, R.C., Luo, L., and Mizrahi, A. (2020). The temporal association cortex plays a key role in auditory-driven maternal plasticity. Neuron 107, 566-579.

Tasker, J.G., and Dudek, F.E. (1993). Local inhibitory synaptic inputs to neurones of the paraventricular nucleus in slices of rat hypothalamus. J Physiol 469, 179–192.

Tirko, N.N., Eyring, K.W., Carcea, I., Mitre, M., Chao, M. V, Froemke, R.C., and Tsien, R.W. (2018). Oxytocin transforms firing mode of CA2 hippocampal neurons. Neuron 100, 593-608.

Uvnas-Moberg, K., Ekstrom-Bergstrom, A., Buckley, S., Massarotti, C., Pajalic, Z., Luegmair, K., Kotlowska, A., Lengler, L., Olza, B., Grylka-Baeschlin, S., Leahy-Warren, P., Hadjigeorgiu, E., Villarmea, S., and Dencker, A. (2020). Maternal plasma levels of oxytocin during breastfeeding — A systematic review. PLoS One 15, 1–38.

Valtcheva, S., and Froemke, R.C. (2019). Neuromodulation of maternal circuits by oxytocin. Cell Tissue Res. 1, 57–68.

Villa, K.L., Berry, K.P., Subramanian, J., Villa, K.L., Berry, K.P., Subramanian, J., Cha, J.W., Oh, W.C., Kwon, H.-B., Kubota, Y., So, P.T.C., and Nedivi, E. (2016). Inhibitory synapses are repeatedly assembled and removed at persistent sites in vivo. Neuron 89, 756–769.

Vithlani, M., Terunuma, M., and Moss, S.J. (2011). The dynamic modulation of GABAa receptor trafficking and its role in regulating the plasticity of inhibitory synapses. Physiol. Rev. 91, 1009–1022.

Wakerley, J., and Lincoln, D. (1973). The milk-ejection reflex of the rat: a 20- to 40-fold acceleration in the firing of paraventricular neurones during oxytocin release. J Endocrinol 3, 477–493.

Wang, J.H., and Stelzer, A. (1996). Shared calcium signaling pathways in the induction of long-term potentiation and synaptic disinhibition in CA1 pyramidal cell dendrites. J. Neurophysiol. 75, 1687–1702.

Wickersham, I.R., Finke, S., Conzelmann, K., and Callaway, E.M. (2007). Retrograde neuronal tracing with a deletion-mutant rabies virus. Nat. Methods 4, 2006–2008.

Xiao, L., Priest, M.F., and Kozorovitskiy, Y. (2018). Oxytocin functions as a spatiotemporal filter for excitatory synaptic inputs to VTA dopamine neurons. Elife 7, e33892.

Xiao, L., Priest, M.F., Nasenbeny, J., Lu, T., Kozorovitskiy, Y., Xiao, L., Priest, M.F., Nasenbeny, J., Lu, T., and Kozorovitskiy, Y. (2017). Biased oxytocinergic modulation of midbrain dopamine systems article biased oxytocinergic modulation of midbrain dopamine systems. Neuron 95, 368-384.

Yasui, Y., Kayahara, T., Nakano, K., and Mizuno, N. (1990). The subparafascicular thalamic nucleus of the rat receives projection fibers from the inferior colliculus and auditory cortex. Brain Res. 537, 323–327.

Zhang, B., Qiu, L., Xiao, W., Ni, H., Chen, L., Wang, F., Mai, W., Wu, J., Bao, A., Hu, H., Gong, H., Duan, S., Li, A., and Gao, Z. (2020). Reconstruction of the hypothalamo-neurohypophysial system and functional dissection of magnocellular oxytocin neurons in the brain. Neuron 109, 331-346.

Acknowledgements

We thank I. Carcea, E. Glennon, K. V. Kuchibhotla, J. K. Schiavo and S. C. Song for comments, discussions and technical assistance. We thank the NYU Langone Microscopy Core for experimental and technical support. We thank D. Rinberg for sharing the custom-made 3D-printed headpost and head-fixation frame design. We thank D. Lin for help with the code for analysis of the fiber photometry data. Initial aliquots of the EnvA G-Deleted Rabies-mCherry (SADΔG-mCherry) and helper AAV2-EF1a-FLEX-TVA-GFP viruses were a gift from G. Fishell. Illustrations in **Figures 1A, 2B, 7D, S3C, and S4A** were made by Shari E. Ross. This work was funded by a Fyssen Foundation Postdoctoral Fellowship, Leon Levy Foundation Postdoctoral Fellowship and Brain & Behavior Research Foundation NARSAD Young Investigator Award (S.V.); a T32 MH019524 Training in Systems and Integrative Neuroscience (H.A.I.); a Natural Sciences and Engineering Research Council of Canada PGS-D fellowship (C.J.B.-M.); an NSF Graduate Research Fellowship (K.A.M.); DP1MH119428 (H.-B.K.); and Program Projects Grant (NS074972), the BRAIN Initiative (NS107616), NICHD (HD088411), NIDCD (DC12557), and a Howard Hughes Medical Institute Faculty Scholarship (R.C.F.).

Author Contributions

S.V. performed in vivo cell-attached, whole-cell and tungsten recordings, fiber photometry, in vitro whole-cell recordings, behavior for chemogenetic inactivation studies, oxytocin sensor experiments, viral injections, histology, image acquisition and data analysis of electrophysiology and behavior experiments. H.A.I. performed fiber photometry and behavior for chemogenetic inactivation studies. C.J.B.-M. performed fiber photometry and in vitro whole-cell recordings for the scrambled dynamin inhibitor experiments. H.A.I., K.A.M., Y.Z. and G.B. wrote code and

performed analysis of the photometry recordings. K.J. and H.-B.K. contributed with design of viral constructs and data analysis for the oxytocin sensor. S.V. and R.C.F. designed the study and wrote the paper.

Declaration of Interests

The authors declare no competing interests.

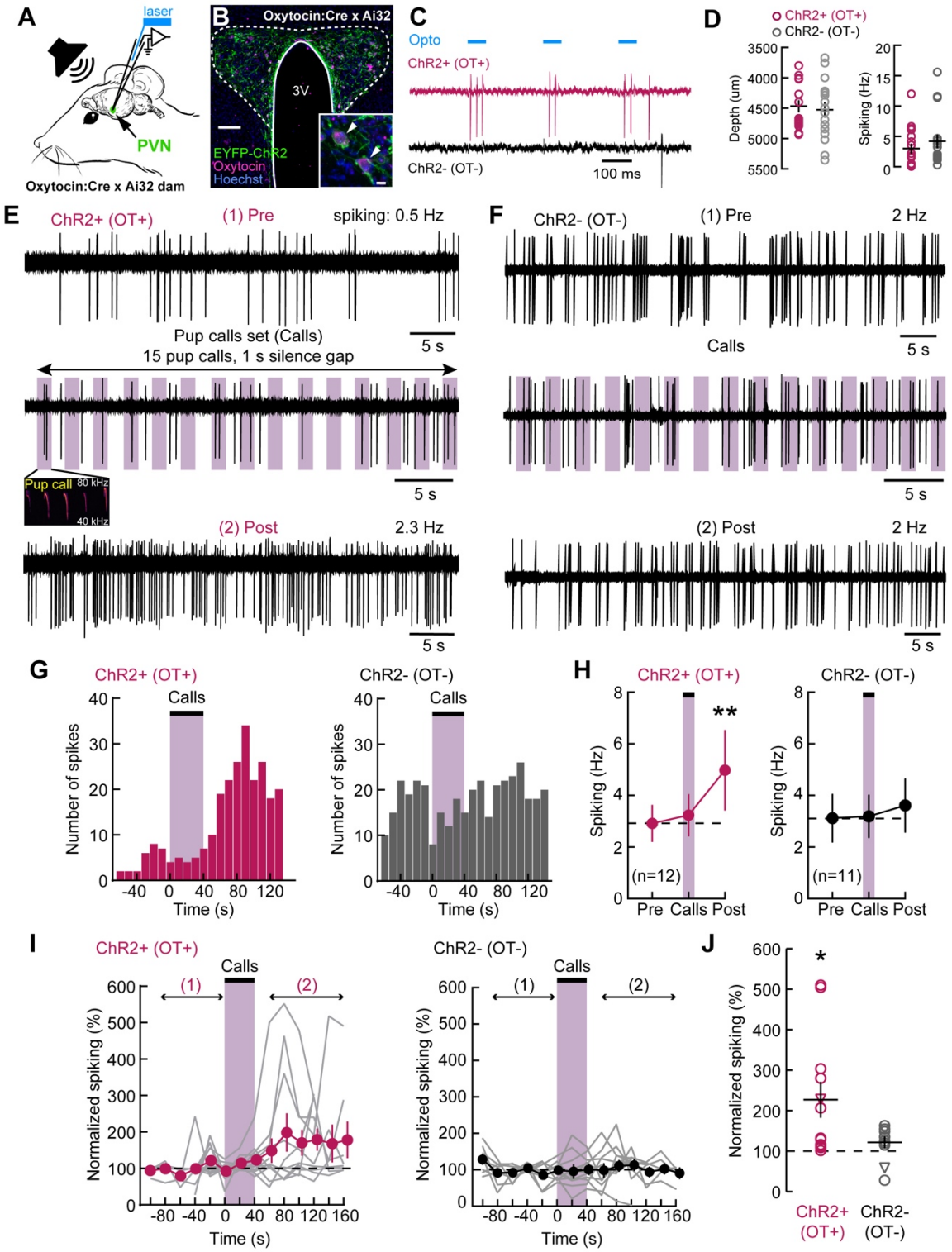

Figure 1 - Valtcheva et al.

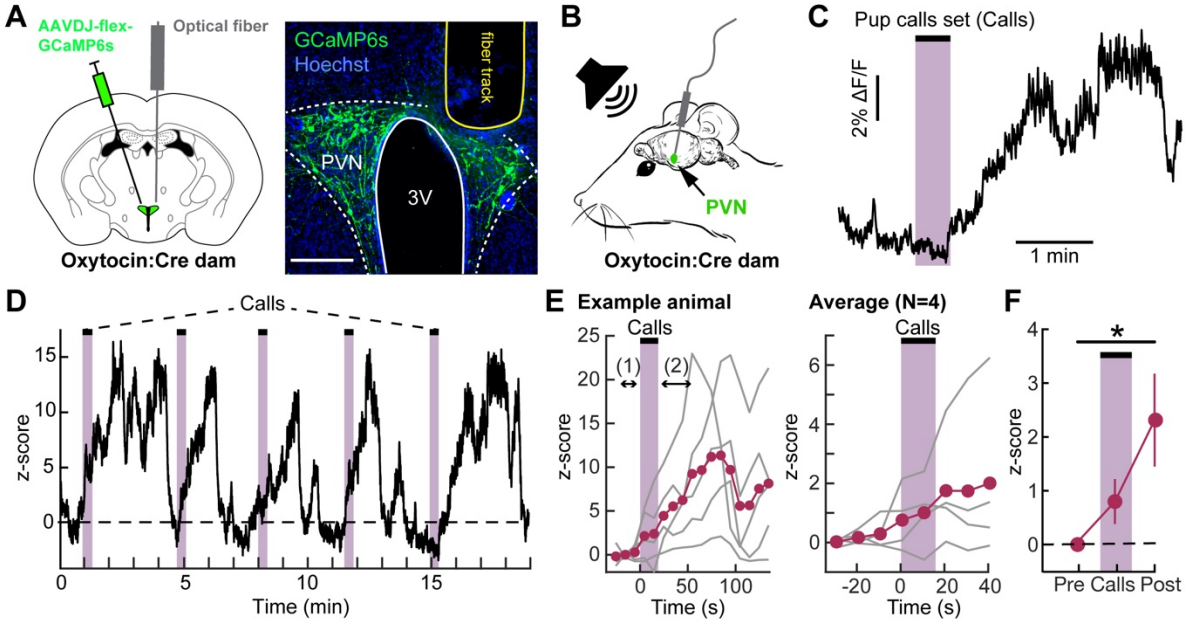

Figure 2 - Valtcheva et al.

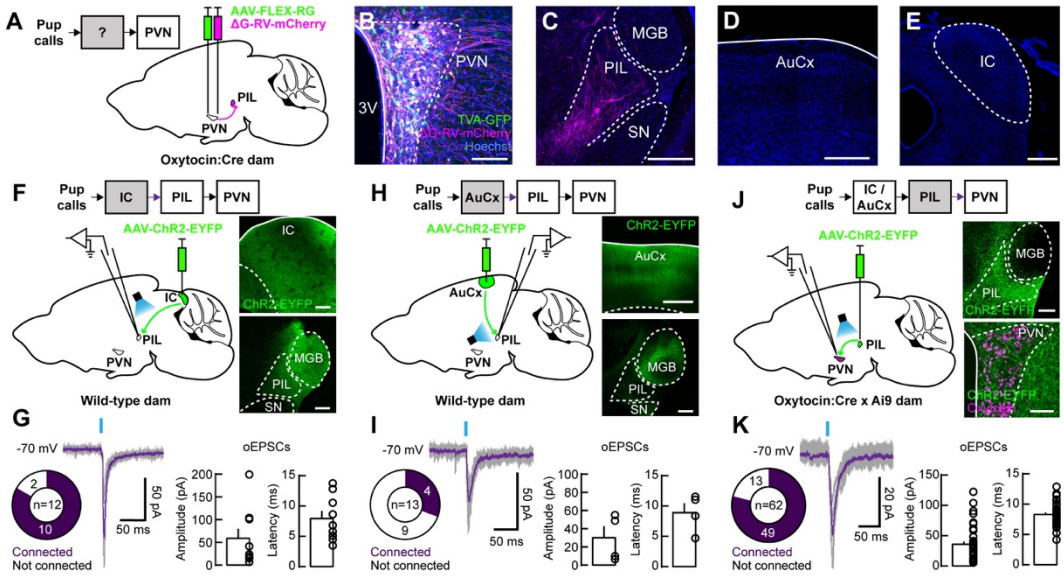

Figure 3 - Valtcheva et al.

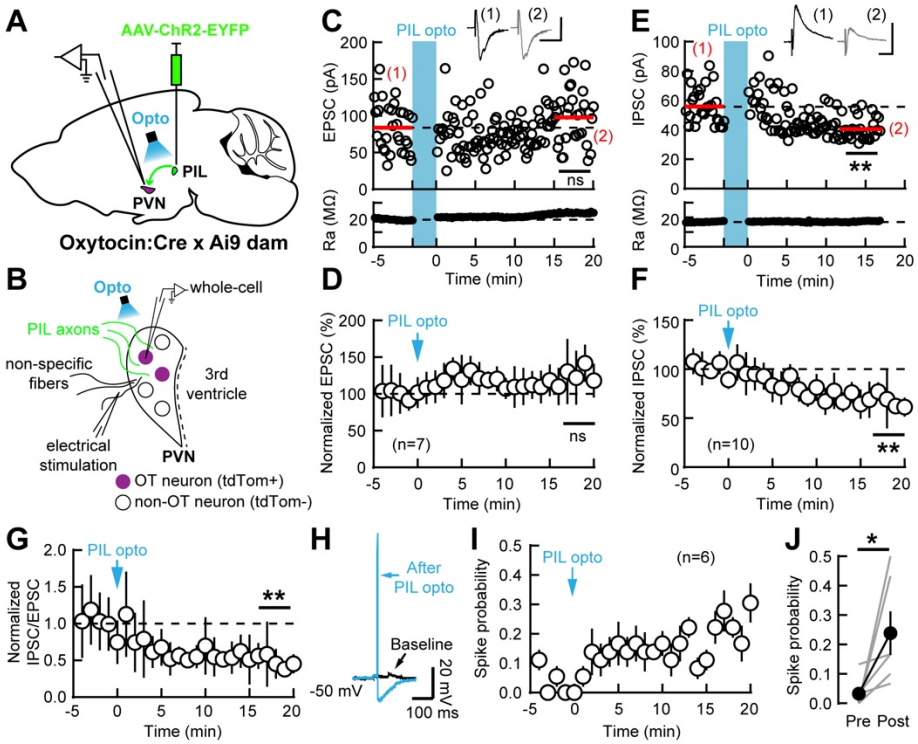

Figure 4 - Valtcheva et al.

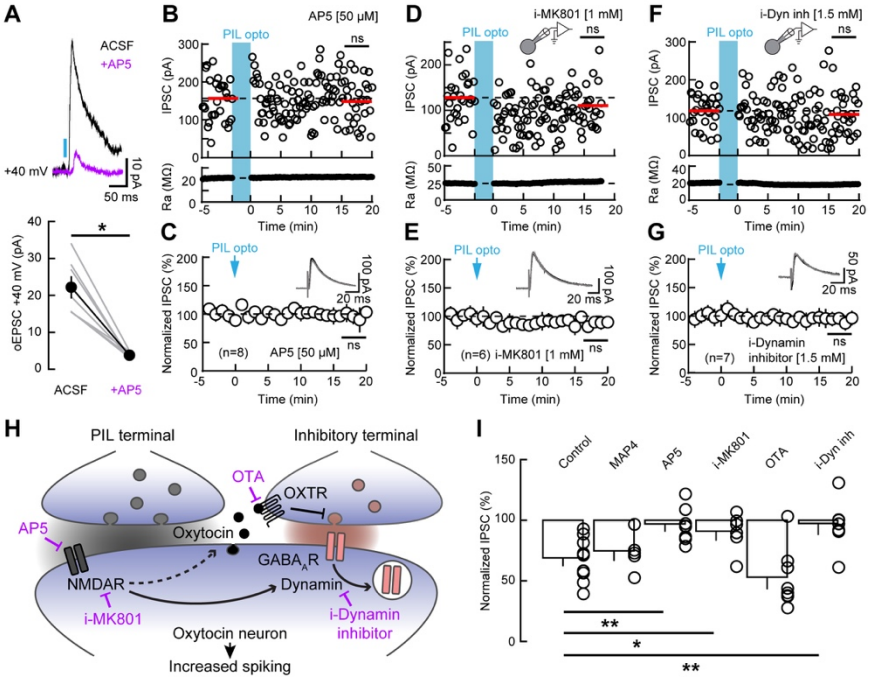

Figure 5 - Valtcheva et al.

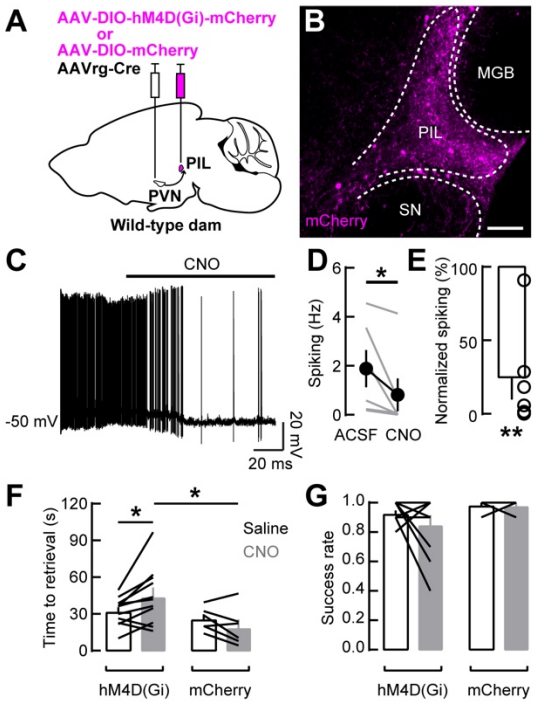

Figure 6 - Valtcheva et al.

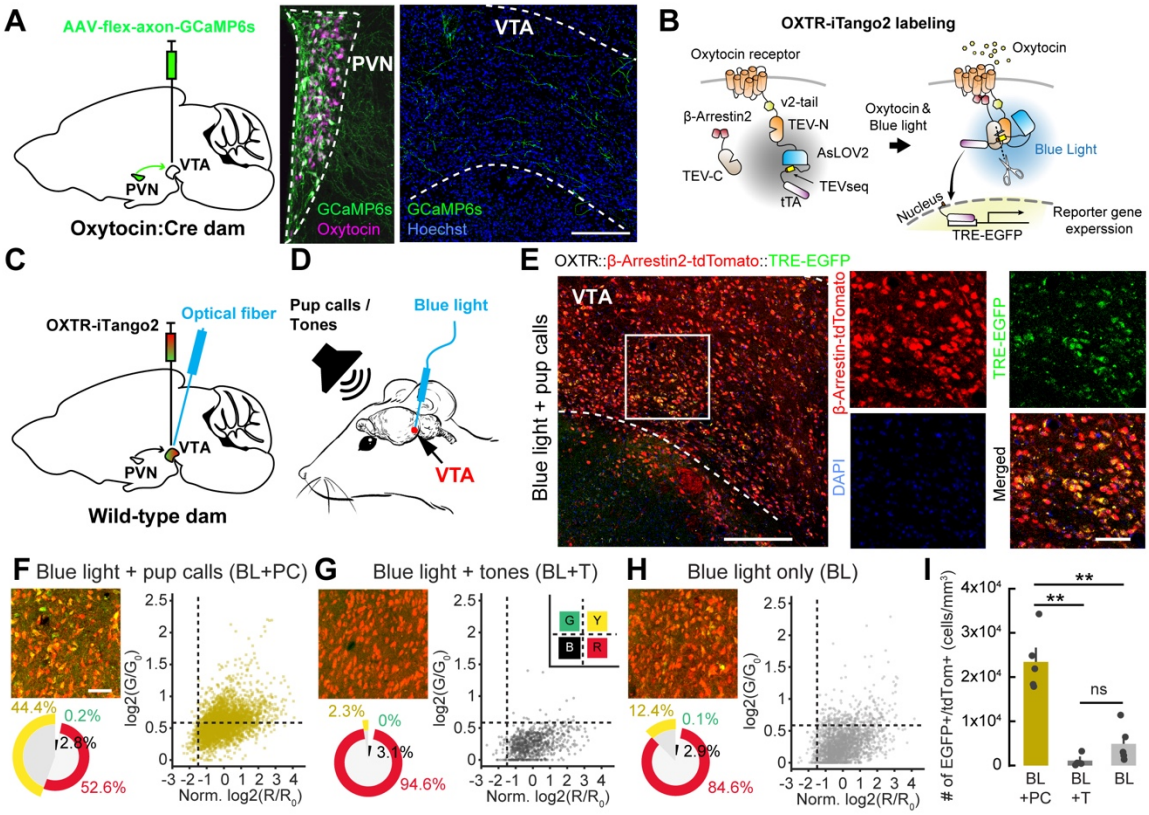

Figure 7 - Valtcheva et al.

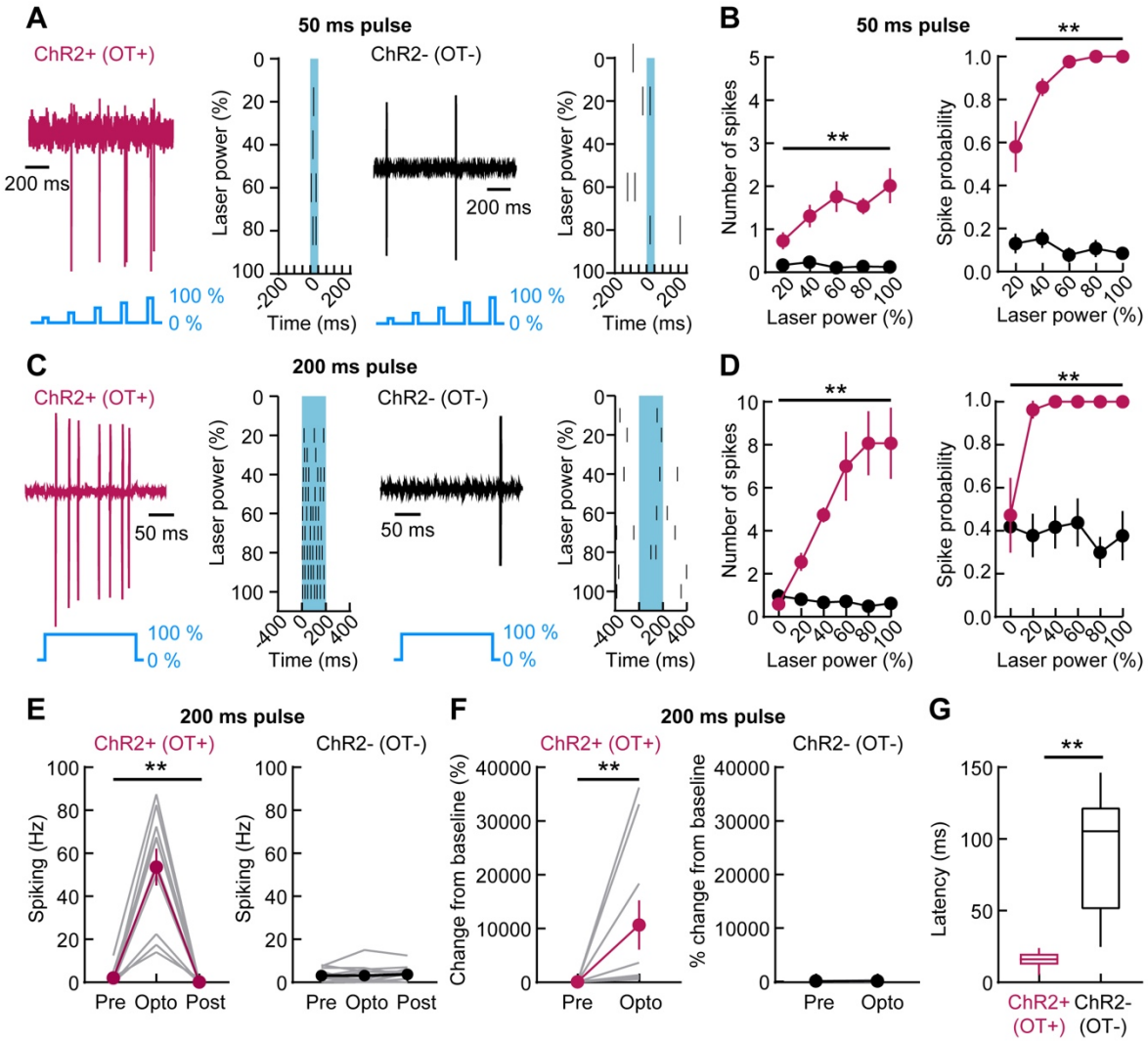

Figure S1 - Valtcheva et al.

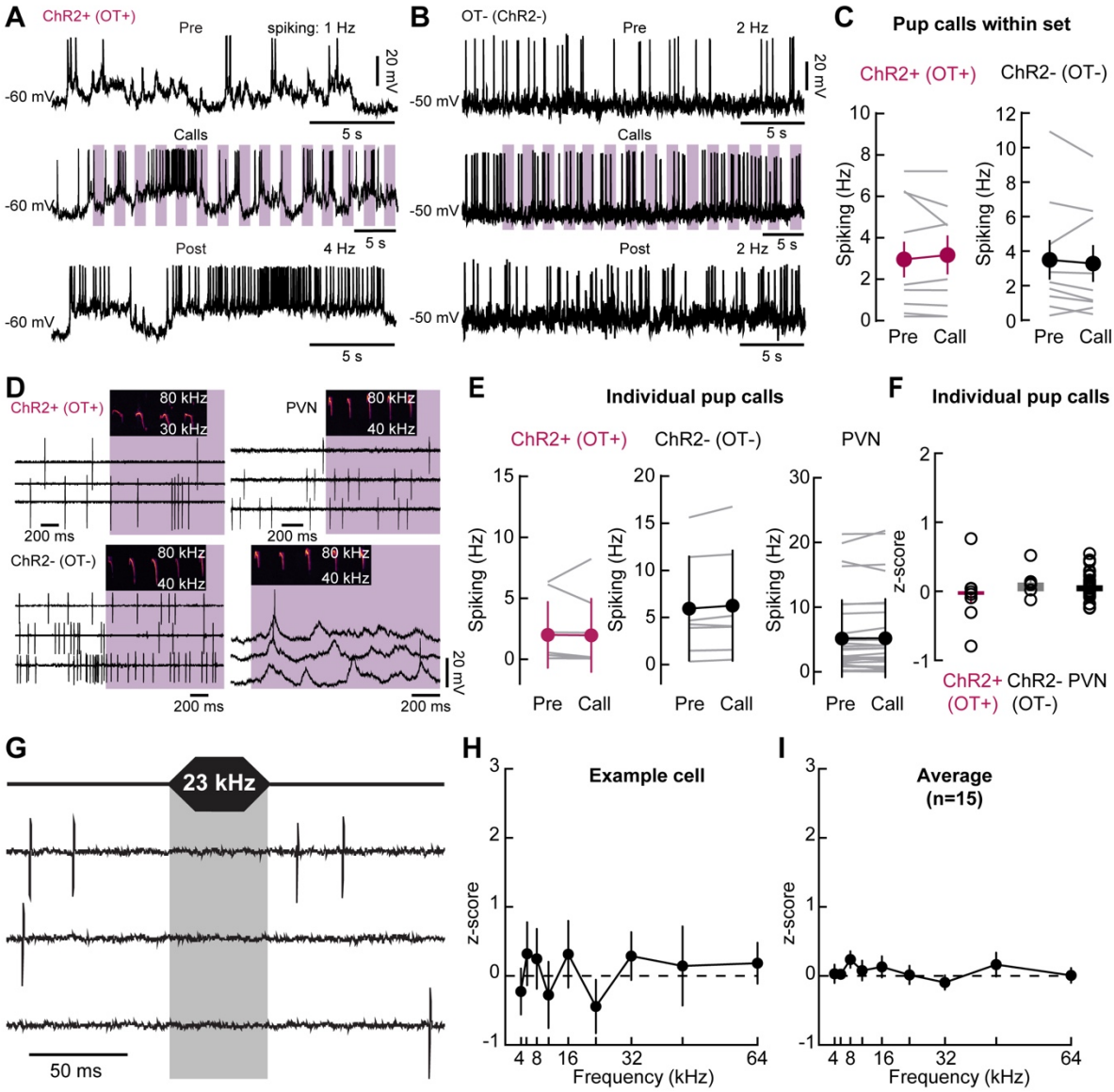

Figure S2 - Valtcheva et al.

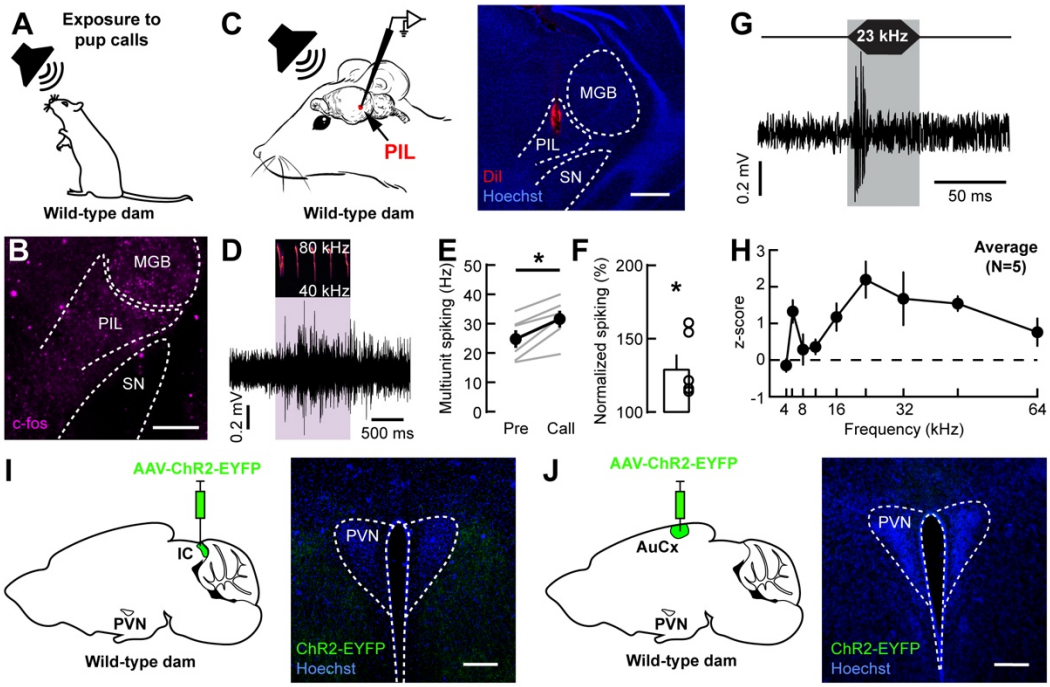

Figure S3 - Valtcheva et al.

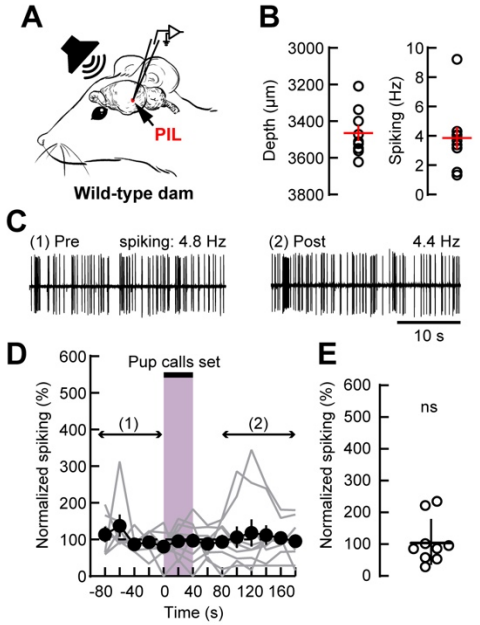

Figure S4 - Valtcheva et al.

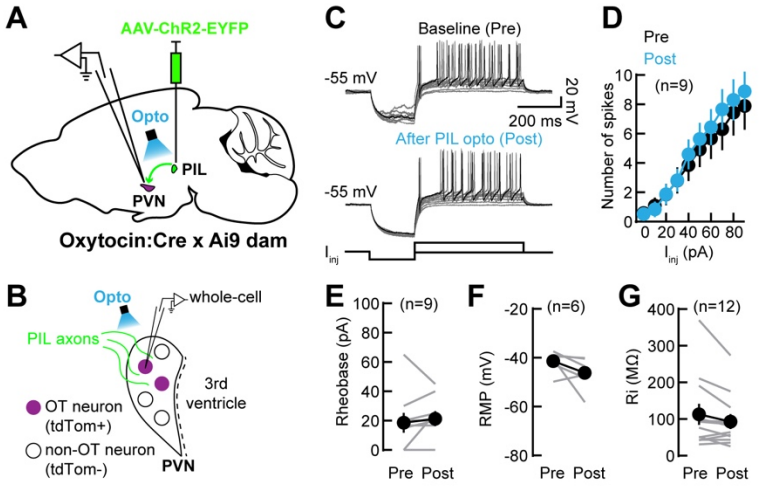

Figure S5 - Valtcheva et al.

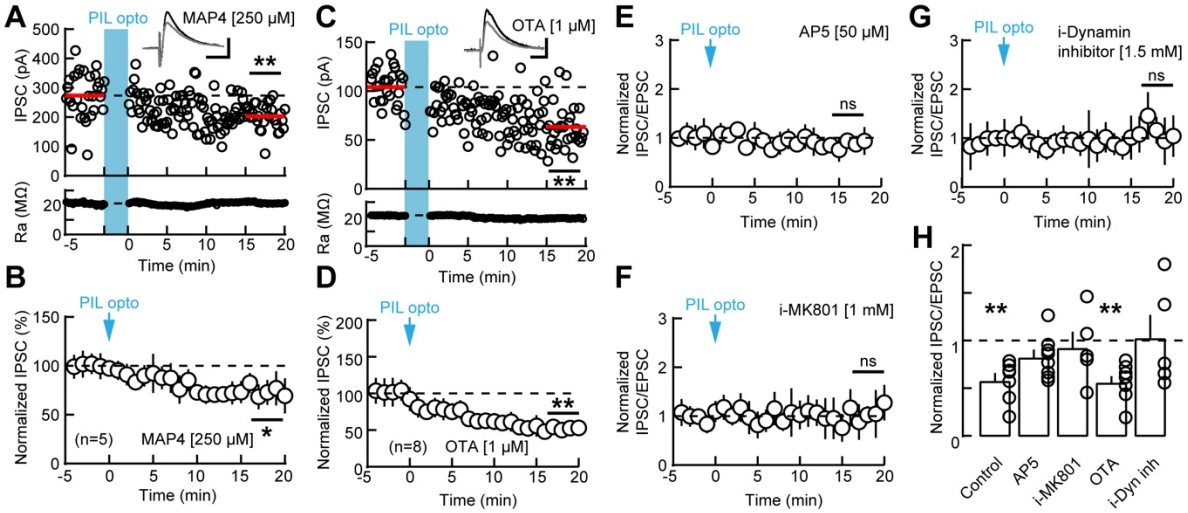

Figure S6 - Valtcheva et al.